

# Mechanism and Evaluation of Hydrogen Permeation Barriers: A Critical Review

Yufan Li, Francesco Barzagli, Peng Liu, Xiaohan Zhang, Zhao Yang, Min Xiao, Yangqiang Huang,\*  
Xiao Luo, Chao'en Li,\* He'an Luo, and Rui Zhang\*



Cite This: *Ind. Eng. Chem. Res.* 2023, 62, 15752–15773



Read Online

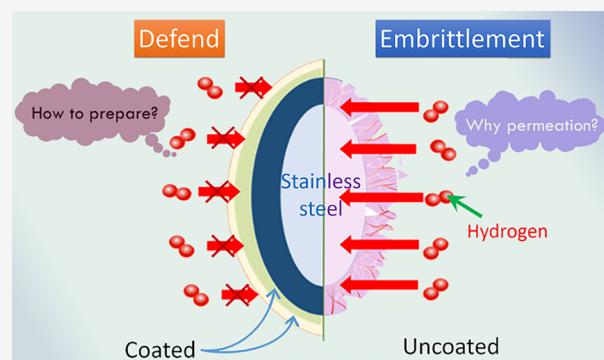
ACCESS |

Metrics & More

Article Recommendations

Supporting Information

**ABSTRACT:** Stainless steel is a common material for high-pressure hydrogen storage. However, the extreme pressure reached in these storage systems accelerates the embrittlement of stainless steel caused by hydrogen, thus reducing its lifetime and seriously limiting the development of the hydrogen industry. Adding hydrogen permeation barrier coatings to the surface of stainless steel is one of the most effective approaches to delay or prevent the permeation of hydrogen and its isotopes through the substrate. Despite the relevance of the issue, studies on hydrogen permeation barrier coating materials have not so far been as popular as those on hydrogen storage materials. In this review, the mechanism of hydrogen permeation and the working principle of hydrogen barriers were investigated. On the basis of this, the hydrogen barrier coatings were classified, the influence factors and defects of the coatings were analyzed, and the preparation technologies along with the methods of evaluation were summarized. Polymer composites strengthened by graphene and other materials were considered more competitive due to their cost effectiveness, better compactivity, and potential for mass production. This review may supply guidance to the further development of hydrogen permeation barrier coating materials.



## 1. INTRODUCTION

The exploration of green technology is a fundamental mission for humanity, and the development of renewable and nonpolluting energy resources has now become a critical challenge, indispensable for guaranteeing a more sustainable future. To address this issue, much attention has recently been focused on hydrogen, one of the most abundant elements in nature, whose oxidation releases three times the energy (per unit mass) of hydrocarbon combustion,<sup>1</sup> and the only product that is generated is water. Today hydrogen is considered an excellent energy vector as it can be generated by electrolysis from renewable sources, and as a clean fuel it could have the potential to replace gas and oil and become the main consumable energy type in the future.

However, some serious limitations of the use of hydrogen comes from its very low energy density (per unit volume) and the consequent need for high-technology solutions for its storage and transport. Different approaches have been developed for the storage of hydrogen in tanks, including extreme gas compression,<sup>2</sup> liquefaction under cryogenic conditions ( $-253\text{ }^{\circ}\text{C}$ ),<sup>3</sup> powder metal adsorption,<sup>4</sup> carbon absorption,<sup>5</sup> etc. Liquefaction consumes an enormous amount of energy to reach the very low temperatures required.<sup>6</sup> Storage with solid-state adsorbents normally needs energy to recover the hydrogen and could not use the pipeline networks for

transportation. Thus, high pressure storage is normally the most convenient storage method for domestic use.

Generally, the hydrogen storage tank is mainly composed of stainless steel or its alloy due to its cost effectivity, maturity of manufacturing, suitability for compressed storage, etc. There normally have four types of hydrogen storage tanks as listed in Table 1.<sup>7–10</sup> The latest hydrogen storage tank are types III and IV: the main body of type III hydrogen storage tank is made of stainless steel or alloy, while type IV (Figure 1) is the polymer liner, coated with different materials, such as a high density polymer liner or carbon fiber composite.<sup>6</sup>

The reason why proper coating is applied in type IV is due to the so-called hydrogen embrittlement, which can make stainless steel fragile and foamy. Hydrogen embrittlement, also known as hydrogen-assisted cracking or hydrogen-induced cracking, is a reduction in the ductility of a metal due to absorbed hydrogen.<sup>11</sup> The embrittlement of a metal is caused by the diffusion of gaseous hydrogen within the material's

Received: July 3, 2023

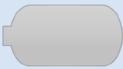



Revised: August 20, 2023

Accepted: August 22, 2023

Published: August 30, 2023



Table 1. Different Types of Hydrogen Storage Tanks

Classification	Type I	Type II	Type III	Type IV
Configuration				
Materials	All metal	Metal liner + (hoop lopped) fibreglass reinforced plastics	Metal liner + (full lopped) carbon reinforced plastics	Polymer liner+ (full lopped) carbon reinforced plastics
Working pressure (MPa)	17.5-20	26.3-30	30-70	> 70
Cost	Low	Medium	High	High
Weight	Heavy	Heavy	Lightweight	Lightweight
Application	For hydrogen stations	For industrial	Vehicular use	Vehicular use with longer life

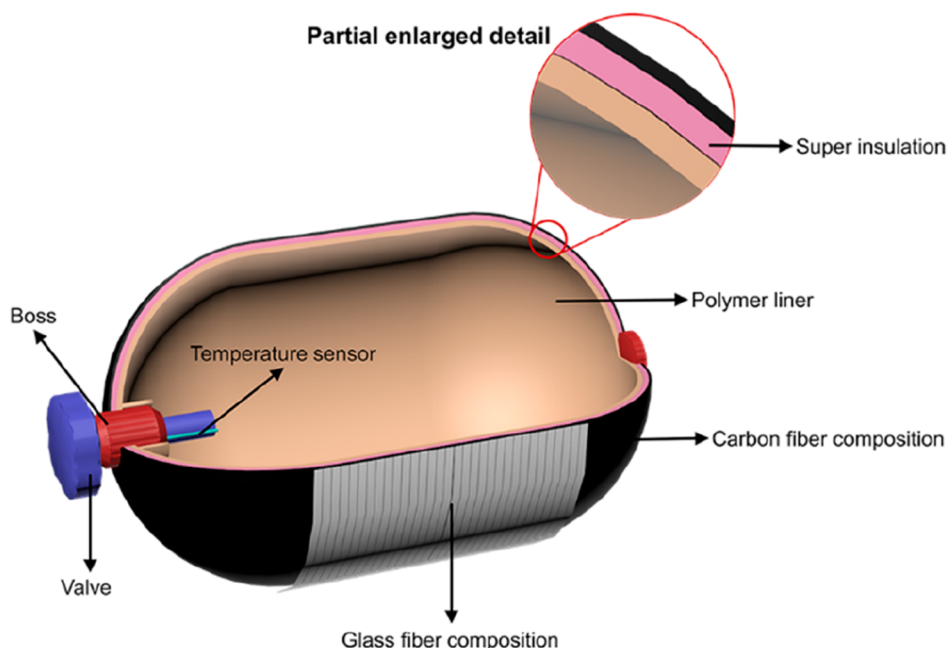


Figure 1. Structure of type IV hydrogen storage tanks.

structure. During the hydrogen diffusion, extreme stress and distortion of the metallic crystal lattice are created, which leads to a reduction of the toughness on the surface of metal materials up to cracking and ultimately results in the leakages of hydrogen and its isotopes, deuterium and tritium.<sup>12,13</sup>

Hydrogen embrittlement is an irreversible phenomenon that must be prevented, as once the damage to the structure occurs, it will be permanent, and it is impossible to do any treatment (Figure 2). As early as the late 1970s, Fowler et al.<sup>14</sup> firstly proposed that the diffusion of hydrogen atoms in stainless steel could be prevented or postponed by depositing hydrogen barrier coating on the surface of stainless steel. The main characteristics that an efficient barrier should possess are (1) the ability to prevent or reduce hydrogen adsorption, (2) a high permeation reduction factor (PRF), and (3) the absence of structural defects such as pores and cracks. However, although it has attracted the attention of researchers, the study

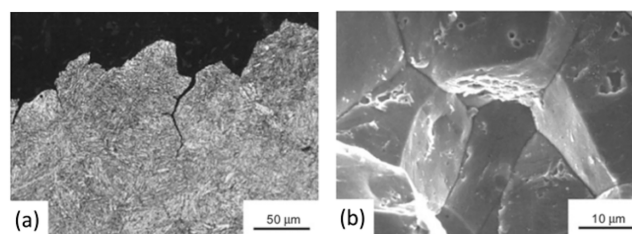


Figure 2. Hydrogen embrittlement occurred on austenitic stainless steel: (a) metallographic section through the fractured surface, showing cracking along prior-austenite grain boundaries of the tempered-martensite structure, and (b) SEM of the fracture surface of a high-strength steel showing brittle intergranular facets. Reprinted with permission from ref 15. Copyright 2011 Elsevier.

on hydrogen permeation barrier coatings nowadays is far behind the investigation on storage materials.

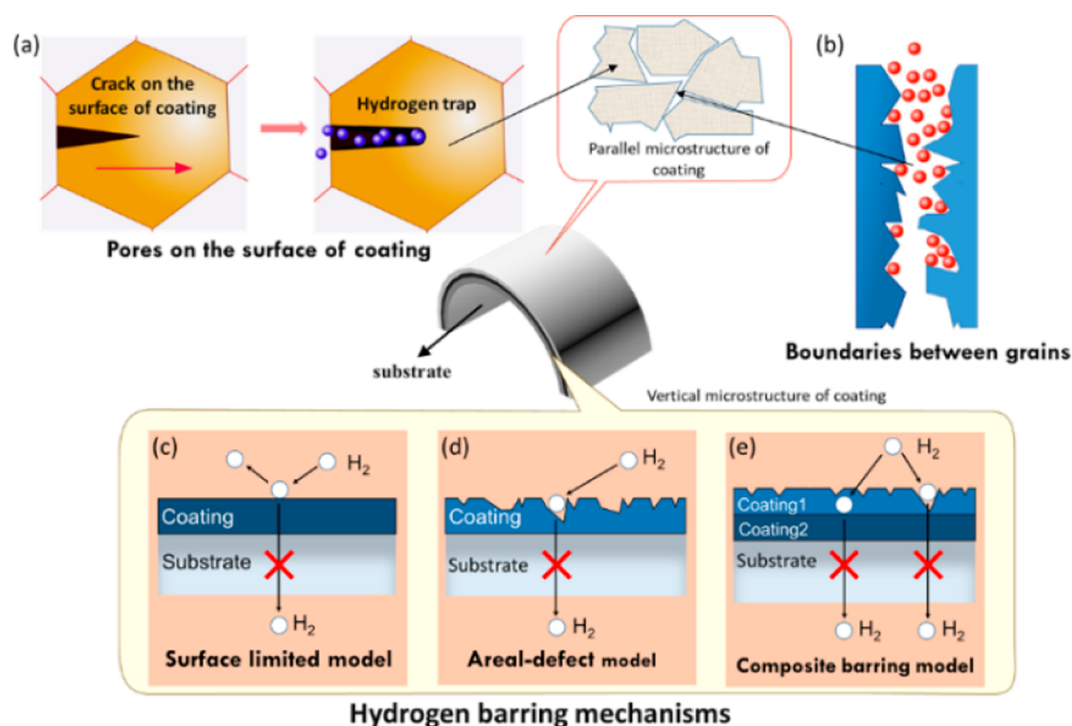


Figure 3. (a,b) Hydrogen molecules are trapped in pores and between boundaries and (c–e) three hydrogen barring models.

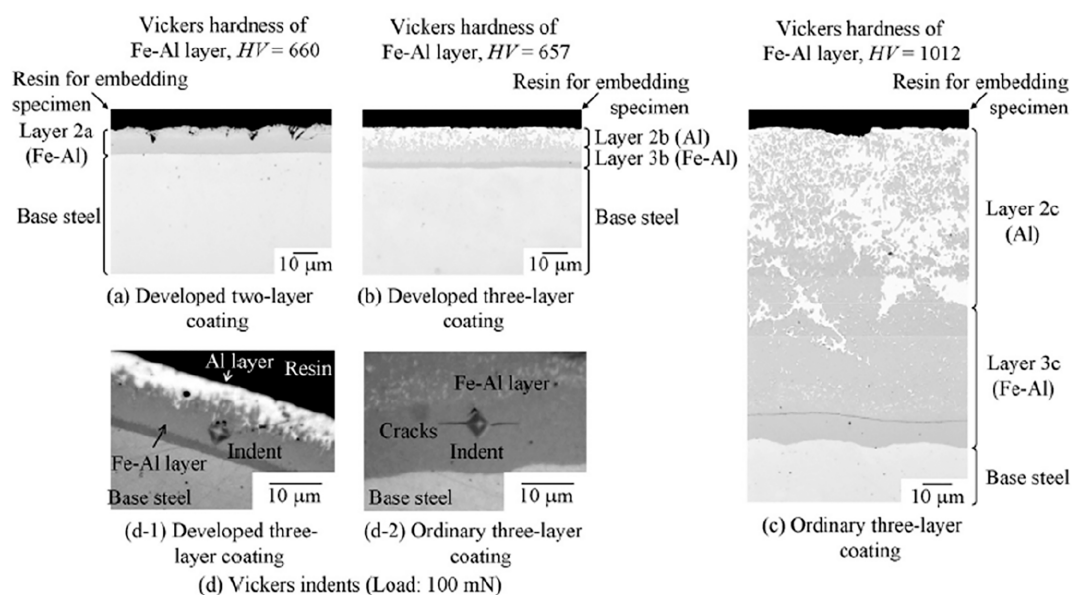


Figure 4. Optical structure of composition hydrogen permeation barrier coating on the base substrate with (a) and (b) are developed two- and three-layered coatings, (c) is the ordinary three-layer aluminum-based coating, and (d-1) and (d-2) inside (d) show Vickers indents on the Fe–Al layer of developed and ordinary three-layered coatings, respectively. Reprinted with permission from ref 23. Copyright 2013 Elsevier.

The hydrogen permeation issue has attracted attention, addition of hydrogen barring coatings as the most cost-effective solution has been proposed, and related reviews are available.<sup>16–22</sup> However, a comprehensive review regarding the most recent development in this area is still necessary. In this review paper, we will try to give a complete overview of hydrogen permeation barriers, examining in detail the following aspects: (1) the investigation of hydrogen permeation models and hydrogen barring mechanisms of different coatings, (2) the classification and exemplification of the

current hydrogen barriers based on the proposed mechanisms, (3) the analysis of the influencing factors, and (4) the consequent discussion on the evaluation methods for assessing the quality of the hydrogen barriers and elaboration of the current problems that need to be overcome.

## 2. HYDROGEN BARRING PRINCIPLES AND BARRIER CLASSIFICATION

**2.1. Hydrogen Barring Principles.** To better understand the hydrogen barring principles, it is necessary to learn the



types of hydrogen permeations. Generally, the study for hydrogen permeation mainly considers two aspects, hydrogen diffusion in which hydrogen diffuses via the pores or cracks of the substrate and hydrogen solution in which hydrogen is dissolved in the substrate, most likely in the atomic state of hydrogen. On the basis of this understanding, three types of hydrogen barring models were proposed: surface limited, areal-defect, and composite barring models,<sup>18</sup> as presented in Figure 3. For the surface-limited model (Figure 3c), the hydrogen permeation is limited by the surface of the coating material. The areal-defect model (Figure 3d) assumes that the hydrogen only permeates part of the coating, and the permeability is a function of the effective contact area of hydrogen. The composite barring model (Figure 3e) normally has multiple hydrogen-resistant modes, such as two-layer (alumina/Fe–Al) and three-layer (alumina/aluminum/Fe–Al) coatings deposited onto cylindrical and pipe (type 304 austenitic stainless steel), prepared by Yamabe et al.<sup>23</sup> The permeation is assumed to occur in the contact area between the coating and hydrogen. The hydrogen resistant ability is mainly determined by the property of the coating material. Among them, the composite barring model (Figure 3e) has been considered as the most widely applied model.

Figure 4 shows the optical micrographs of the coating with a three-layer composite structure, where panels a and b show developed two- and three-layered coatings obtained with the specially blended aluminum alloy, panel c is the three-layer aluminum-based coating obtained with an ordinary pure aluminum, and panels d-1 and d-2 show indents on the Fe–Al layer of developed and ordinary three-layered coatings with the Vickers hardness (HV) = 657 and 1012, respectively.

It is noted that the hydrogen penetration through the metal or its alloy is believed to be in the form of dissociated hydrogen atoms.<sup>18</sup> However, the main purpose of hydrogen barring coatings is for blocking the diffusion of hydrogen molecules.

**2.2. Calculation of Hydrogen Permeability.** As stated above, Figure 3 shows the working principles of the hydrogen-resistant coatings. It is noted that the hydrogen permeation through the bulk of metal substrates normally occurs via the diffusion of hydrogen atoms rather than in the state of hydrogen molecules.

In accordance with the study related to hydrogen permeation through a PdCu membrane,<sup>24</sup> the rate of migration of hydrogen through the layers of a planar membrane is limited by the diffusion of the H atoms in the bulk of the substrate, since the adsorption, dissociation, recombination, and desorption processes on the surface are rapid. Thus, the mechanism for barring the hydrogen permeation can be considered from constraining the H atom diffusion in the bulk of the substrate. Hence, limiting the diffusion of H atoms in the substrate can be considered as a possible mechanism to block hydrogen permeation.

Two distinguishable permeation mechanisms related to the hydrogen transport regime are introduced depending on the upstream hydrogen pressures: the diffusion-limited regime (DLR) in which bulk diffusion controls the kinetics and the surface-limited regime (SLR) in which surface reactions govern the process.<sup>25</sup>

In accordance with the diffusion-limited regime (DLR) mechanism, the surface processes are assumed so fast that Sieverts' equilibrium is always reached regardless of net mass flow and the diffusion in the solid is the determining kinetic

parameter.<sup>26</sup> The Sieverts' law (eq 1) states that the solubility of a diatomic gas such as hydrogen in metal is proportional to the square root of the partial pressure of hydrogen in thermodynamic equilibrium:<sup>27</sup>

$$C_{\text{in}} = \sqrt{K \times P} \quad (1)$$

where  $C_{\text{in}}$  is the concentration of the dissolved hydrogen atoms into the metal,  $K$  is the equilibrium constant, and  $P$  is the hydrogen partial pressure on the interface with the metal.

In accordance with the surface-limited regime (SLR) mechanism, the adsorption and recombination processes are decisive for the kinetics;<sup>26</sup> moreover, this mechanism can be further divided into an outlet surface-limited regime (OLR) and inlet surface-limited regime (ILR) when the surface conditions on the two sides of the membrane are different (asymmetric membrane).<sup>28</sup>

Usually the diffusion-limited regime is applied in materials softer in the inlet side and more rigid on the outlet side, while the surface-limited regime is applied in those softer on the outlet side and more rigid in the inlet side.<sup>29</sup> So, in the DLR mechanism, the goal is to produce a hydrogen trap through many vacancies in the material to capture the hydrogen atoms during permeation; carbides and nitrides are this type of coating materials. In the SLR mechanism, on the other hand, the aim is to keep the hydrogen atom out of the substrate through intensive metal bonds, atomic bonds, and crystal structures such as to reduce the permeability. Hydrogen permeability can be measured with the so-called hydrogen permeation reduction factor (PRF, the definition is given in section 4.2.2), which is the ratio of the permeabilities between the bare and the coated substrates. The related bond energies are listed in Table 2. This kind of barrier is mainly represented by metal and metal oxides.

**Table 2. Chemical Bond Energies of Typical Materials**

bond	Si–H	C–H	N–H	O–H
bond energy (kJ/mol)	318	411	386	459

The surface limited regime (SLR) is normally applied at low pressures, but the experimental evaluation of the efficiency is difficult. In the diffusion limited regime (DLR), it is assumed that all processes are thermally activated and can be described with the Arrhenius equation (eq 2). The diffusion process in any layer is described by the diffusion coefficient  $D$ , whose exponential dependence on temperature is specified by the pre-exponential term  $D_0$  and the diffusion activation energy  $E_D$ .<sup>30</sup>

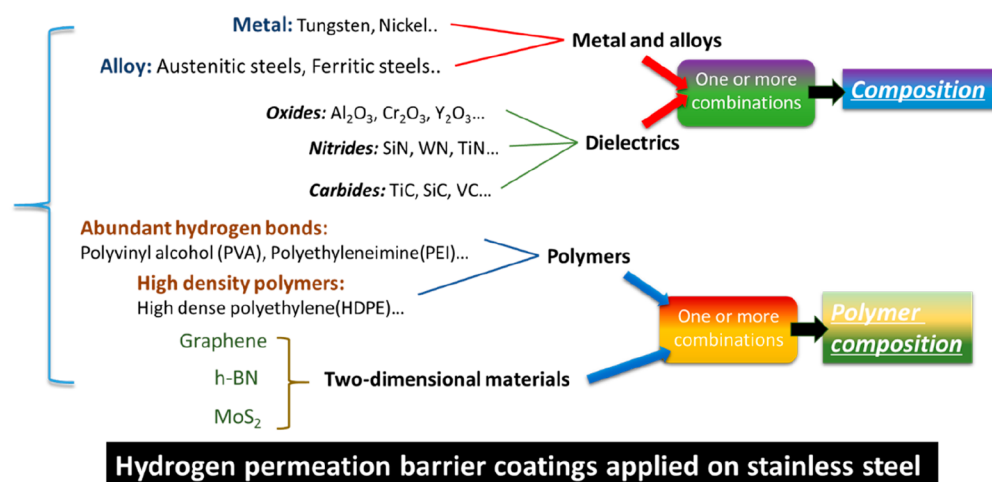
$$D = D_0 \exp\left(-\frac{E_D}{RT}\right) \quad (2)$$

It should be noted that most reported evaluation data for hydrogen permeation barriers were tested under high pressure and temperature, so the DLR may not be suitable in all cases.

**2.3. Classification of Hydrogen Permeation Barriers.** Hydrogen permeation barriers include metal and alloys, dielectrics, polymers, two-dimensional materials, etc., as showed in Figure 5. Different coatings and their performances as hydrogen barriers are summarized in Table S1.

**2.3.1. Metals and Alloys.** Generally, most metals and metal alloys exhibit a certain hydrogen barring effect, as shown in Table 3, where the hydrogen permeability ( $P_m$ ) is expressed as mol H<sub>2</sub>/(m s Pa<sup>0.5</sup>). However, the application of metals and





### Hydrogen permeation barrier coatings applied on stainless steel

Figure 5. Classification of hydrogen permeation barriers.

Table 3. Hydrogen Permeability of Several Metals and Metal Compounds at 400–500 °C<sup>17,25</sup>

materials	$P_m$ [mol H <sub>2</sub> /(m s Pa <sup>0.5</sup> )]	T (°C)	comments
vanadium	$2.9 \times 10^{-8}$	500	extremely sensitive to surface oxides
niobium	$7.5 \times 10^{-9}$	500	–
titanium	$7.5 \times 10^{-9}$	500	stable hybrids
iron	$1.8 \times 10^{-10}$	500	–
nickel	$1.2 \times 10^{-10}$	500	–
ferritic steels	$3 \times 10^{-11}$	500	–
austenitic steels	$0.9$ to $1.2 \times 10^{-11}$	500	large data compilation
molybdenum	$1.2 \times 10^{-11}$	500	variable
tungsten	$4.3 \times 10^{-15}$	500	extrapolated from high <i>t</i> test
beryllium	$2 \times 10^{-15}$	400	–
titanium carbide	$\sim 1$ to $8 \times 10^{-15}$	500	external physical vapor deposition coating
titanium carbide/ titanium nitride, layered	$\sim 7 \times 10^{-16}$	500	external physical vapor deposition coating
aluminum oxide	$\sim 9 \times 10^{-17}$	500	extrapolated from high <i>t</i> tests
Beta-SiC	$\sim 1 \times 10^{-20}$	500	extrapolated

alloys as hydrogen permeation barriers is constrained by the harsh manufacturing conditions.<sup>25</sup> For example, beryllium (Be) is produced by hot pressing metallurgy under high pressure. The grain size is hard to control, and therefore, the hydrogen barrier effect is difficult to keep homogeneous. Tungsten (W) has a hydrogen permeability of only  $4.3 \times 10^{-15}$  mol H<sub>2</sub>/(m s Pa<sup>0.5</sup>) at 500 °C (Table 3), but it is manufactured in very harsh operating conditions, in a fusion reactor at an extremely high temperature above 3410 °C.<sup>25</sup> It is noted that the power of pressure is 0.5, which means hydrogen permeation via the atomic state. The permeation of hydrogen is either in the atomic or molecular form. The former is normally the case where hydrogen is dissolved in metal materials, while the latter is sometimes the case where the permeation is through nonmetal materials, which will be described in detail in section 4.2.2.

Although tungsten retains strength at elevated temperatures, higher than the melting point of 3410 °C, and has low

hydrogen diffusion compared to other metals, it still undergoes hydrogen embrittlement.<sup>31</sup> Hence, regarding the reaction with hydrogen, the stability of the surface quality, the obvious hydrogen permeability, the environmental protection, and the cost, pure metals are clearly not enough to meet the hydrogen-resistance requirements. The coating currently used to minimize the hydrogen diffusion into and through the substrate of nuclear thermal propulsion engines is tungsten deposited on UO<sub>2</sub> spheres via chemical vapor deposition (CVD) before they are embedded in the metallic matrix.

**2.3.2. Dielectrics Compounds.** **2.3.2.1. Oxides.** Oxides are always present on the surfaces of most metals. The hydrogen permeation-resistant behaviors of different oxides differ from each other due to the different atomic structures. The advantage of using oxides is that they can simply form while exposed to air.

**Alumina (Al<sub>2</sub>O<sub>3</sub>).** Al<sub>2</sub>O<sub>3</sub> has great self-healing ability and chemical stability. In particular,  $\alpha$ -Al<sub>2</sub>O<sub>3</sub> has an intensive octahedral structure with excellent resistance to hydrogen permeation.<sup>32</sup> Alumina-deposited coatings have been used for various applications.

However, the super hydrogen permeation resistance and the thermodynamical stability of alumina ( $\alpha$ -Al<sub>2</sub>O<sub>3</sub>) are only guaranteed at high temperature (above 900 °C). Consequently, it can only be combined on metals that support heat treatment at a temperature equal or higher than 900 °C, which restricts the field of application on some steels. On the other hand, the thermal expansion coefficient (TEC) of Al<sub>2</sub>O<sub>3</sub> is  $7.5 \times 10^{-6}$  K<sup>-1</sup>, very different from more conventional substrates (such as in 316L steel, with TEC of  $19.6 \times 10^{-6}$  K<sup>-1</sup>). Therefore, cracking and sloughing off may occur during annealing and use.

There are two approaches to overcome these drawbacks: (1) consider replacing  $\alpha$ -Al<sub>2</sub>O<sub>3</sub> with compounds of similar shape and performance and (2) use composites, like the Cr<sub>2</sub>O<sub>3</sub>/Al<sub>2</sub>O<sub>3</sub> bipolar oxides, as hydrogen permeation barriers. For example, Ramm et al.<sup>33</sup> prepared the Al–Fe–O hydrogen permeation barrier with an octahedral structure similar to  $\alpha$ -Al<sub>2</sub>O<sub>3</sub> through physical deposition. Instead, Zhang et al.<sup>34</sup> deposited Al<sub>2</sub>O<sub>3</sub> on a Cr<sub>2</sub>O<sub>3</sub> layer by atomic layer deposition (ALD). The Cr<sub>2</sub>O<sub>3</sub> layer was generated by the preoxidization of stainless steel at 550 °C with cyclic voltammetry (CV).

**Chromia ( $Cr_2O_3$ ).** Chromium oxide has a high bond strength with the substrate, and it is usually used as an intermediate layer of a coating.<sup>35</sup> The permeation reduction factor of  $Cr_2O_3$  can reach 1000 at 700–800 °C, related to pure chromium.<sup>36</sup> As a key component on the stainless-steel surface,  $Cr_2O_3$  can effectively inhibit the oxidation of the bulk metal.

Mixtures of chromium and aluminum have extremely high permeation reduction factors. Levchuk et al.<sup>37</sup> deposited the Al–Cr–O film on Eurofer 97 steel by filtrating arc discharge technology at 700 °C, reaching the permeation reduction factor in the range of 2000–3500.

**Erbium Oxide ( $Er_2O_3$ ).** Levchuk et al.<sup>38</sup> reported that  $Er_2O_3$  has a crystal structure similar to  $\alpha-Al_2O_3$ , which can efficiently inhibit the diffusion and reduce the permeation of hydrogen.

**Yttria ( $Y_2O_3$ ).** Considering the high cost of erbium oxide, yttria was proposed as a substitute for  $Er_2O_3$  in nuclear reactors. Yttria was often used at the high temperatures around 700 °C.<sup>39</sup> Yttria has high thermal and chemical stability, low activation, and a high hydrogen isotope permeation reduction factor, which is more promising than  $Er_2O_3$  for larger scaled applications.

Chikada et al.<sup>39</sup> obtained the  $Y_2O_3$  coating on the reduced activation ferritic/martensitic steel F82H; the resulting permeation reduction factor ranged from 100 to 390. Wu et al.<sup>40</sup> reported permeation reduction factor values between 240 and 410 using metal organic chemical vapor deposition (MOCVD) on the surface of stainless steel 316L. The reason why wide ranges are reported is because the quality of  $Y_2O_3$  is controlled by both diffusion and the characteristics of the coated surface.

Both erbium and yttrium are rare earth elements. As rare earth resources are scarce, the costs of the related coatings are high and not suitable to wide domestic usages.

**Zirconia ( $Zr_2O_3$ ).**  $Zr_2O_3$  is a much cheaper material. The hydrogen resistance of  $Zr_2O_3$  is more stable, and that does not change with temperature.  $Zr_2O_3$  exhibits a high surface density and binding degree, however, it requires a high quality preparation process as well.

Hatano et al.<sup>41,42</sup> recoated zirconia using an electrolytic deposition method to fill the holes of existing zirconia coating which was produced with the sol–gel method on a Cr–Fe alloy substrate. The permeation reduction factor is higher than 1000 at the temperature between 300 and 500 °C.

**2.3.2.2. Nitrides. Titanium Nitride (TiN).** Titanium nitride and carbide (TiC) often form composite coatings. Compared to titanium carbide, the surface of the nitride is denser. Titanium nitride has better hydrogen resistance and more potential than the pure carbide.<sup>18</sup> The TiN–TiC layer has an advantage in reliable adhesion. Therefore, it can be used as an adhesive layer like  $Cr_2O_3$  on some composite barriers.<sup>43</sup>

Wang et al.<sup>44</sup> prepared a double layer structure coating through the filling cementation method. The outer layer is titanium nitride, while the inner layer is a diffusion layer, from titanium atoms to the matrix. After nitriding and oxidation processes, the coating becomes  $TiO_2$  (with the rutile structure) on the outer layer, TiN in the middle, and TiC on the inner surface. The  $TiO_2$ –TiN–TiC barrier can reduce the steady-state hydrogen permeation to 0.7% of the substrate value alone.

Checchetto et al.<sup>45</sup> obtained a TiN–TiC bilayer through ion beam assisted deposition (IBAD) on the surface of martensitic stainless steel. The hydrogen permeability is 4 orders of magnitude less than that of the substrate itself. However, TiN–

TiC bilayer has low surface density and is easily cracked, making it difficult to use for hydrogen-resistance purposes.

**Silicon Nitride ( $SiN/Si_3N_4$ ).** The requirement for the quality of the substrate on which silicon nitride is coated is relatively high. If the silicon nitride barrier does not match the substrate, cracks and holes will form on the surface of the film, so the permeation reduction factor will be greatly reduced. It was found that the high hydrogen permeability resulted from the hydrogen present in the substrate before the deposition, for example, Nemanič et al.<sup>46</sup> prepared a silicon nitride barrier on ferrite stainless steel by radio frequency sputtering, reaching a permeation reduction factor of over 2000. Therefore, it is important to keep the surface of the substrate clean. Hydrogen is also dissolved during annealing. However, the hydrogen-resistant mechanism of silicon nitride is still under research.

**Tungsten Nitride (WN).** The tungsten coatings are easily cracked during thermal annealing due to the difference in thermal expansion coefficient with substrates. The advantages for tungsten nitride and the WN–W composite coatings are no degradation under thermal annealing and suitability as the tritium permeation barrier on steel. The permeation reduction factor of tungsten nitride is 2 orders of magnitude higher than the noncracked tungsten layer under the applied pressure and temperature range.<sup>49</sup>

**Boron Nitride (BN).** The characteristic of boron nitride is determined by its structure. The common structures present during the preparation of hydrogen permeation blocking coatings are amorphous, cubic, hexagonal, and turbostratic, indicated as *a*-, *c*-, *h*-, and *t*-BNs, respectively. Among them, the *c*-BN has a diamondlike structure, which gives a very high hardness (second only to diamond). *c*-BN has a  $sp^3$ -bonded phase, while the *h*-BN has a  $sp^2$ -bonded phase like graphene,<sup>48</sup> which will be introduced in section 2.3.4.

**2.3.2.3. Carbides. Silicon Carbide (SiC).** Silicon carbide material has advanced heat resistance, hardness, and surface density.

Qamar et al.<sup>49</sup> prepared hexagonal silicon carbide thin films at different temperatures and deposition rates through radio frequency reactive magnetron. The dense silicon carbide film was formed on a silicon surface within the temperature range of 850–950 °C. Wang et al.<sup>50</sup> prepared silicon carbide films on stainless steel 316L using both ion beam-assisted deposition and ion implantation methods. In this way, the permeation reduction factor reached the astonishing value of 10000. Wu et al.<sup>51</sup> obtained silicon carbide film on stainless steel 316L through magnetron sputtering, and Chikada et al.<sup>52</sup> prepared it on ferritic/martensitic steel F82H. The resulting permeation reduction factors were 200 and 1000, respectively.

Compared to other materials, silicon carbide shows excellent hydrogen resistant ability due to its high density. However, like alumina, the disadvantage of silicon carbide film is easy cracking due to the different thermal expansion coefficients between the coating and the substrate steel.

**Vanadium Carbide (VC).** The difference between vanadium carbide and other traditional materials is that the effect of hydrogen permeation in VC occurs mainly on the surface. It has super plasticity, high temperature stability, and a proper thermal expansion coefficient for stainless steel. The hydrogen permeation barrier of vanadium carbide is equivalent to the traditional  $\alpha-Al_2O_3$  hydrogen permeation coating.<sup>53,54</sup>

**2.3.3. Polymers.** The principle for polymers to prevent hydrogen is based on the “like dissolving like” principle, whereby polar substances tend to be dissolved in polar solvents

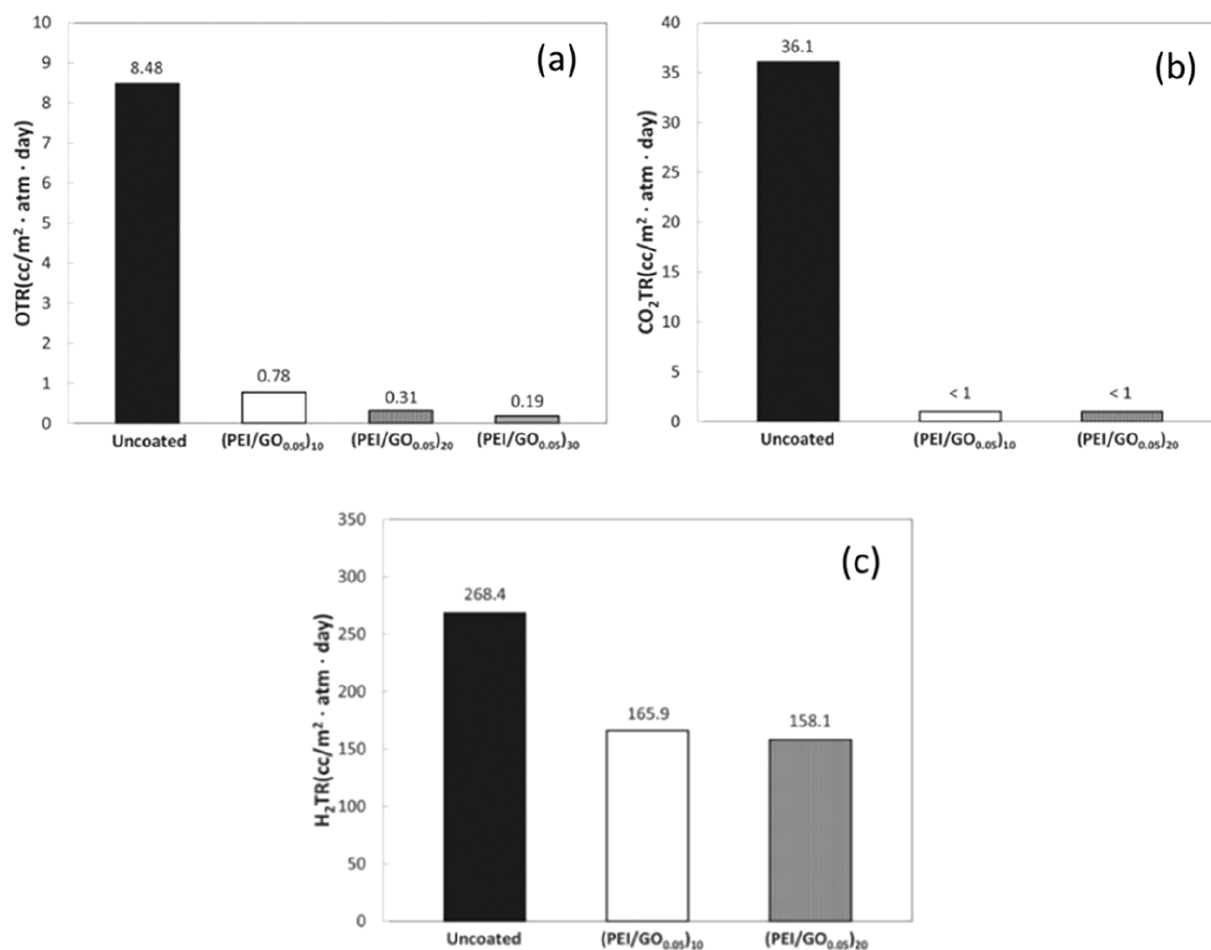


**Figure 6.** Transmission rates of O<sub>2</sub> (OTR, a), CO<sub>2</sub> (b), and H<sub>2</sub> (c) through polyethyleneimine (PEI)/graphene oxide (GO) assembled and uncoated polyethylene terephthalate (PET). Adapted with permission from ref 61. Copyright 2013 Wiley-VCH.

and nonpolar substances prefer nonpolar solvents.<sup>55</sup> Since hydrogen is a nonpolar molecule, it prefers to be dissolved in nonpolar solutions.

The group polarities in organic materials such as polymers vary in the following order:<sup>55</sup> alkanes (–CH<sub>3</sub>, –CH<sub>2</sub>–) < alkenes (–CH=CH–) < ethers (–O–CH<sub>3</sub>, –O–CH<sub>2</sub>–) < nitro-compounds (–NO<sub>2</sub>) < dimethylamines (CH<sub>3</sub>–N(R)–CH<sub>3</sub>) < lipids (–COOR) < ketones (–CO–) < aldehydes (–CHO) < mercaptans (–SH) < amines (–NH<sub>2</sub>) < amides (–NHCO–CH<sub>3</sub>) < alcohols (–OH) < phenols (Ar–OH) < carboxylic acids (–COOH).

Polymer materials can severely limit the diffusion of hydrogen when they have a very compact structure. Copolymers of poly(vinylidene fluoride) (PVDF), polyester, polyamide (PA), and ethylene vinyl alcohol (EVOH) have been reported to be appropriate materials for hydrogen resistance. Materials like poly(vinyl alcohol) (PVA), rich in hydroxyl groups, have good hydrogen resistance since the hydrogen bonds between poly(vinyl alcohol) molecular chains make the polymer very compact and, hence, with very few channels for hydrogen passing.<sup>56</sup>

However, the use of such polymers has some limitations. Polyester and polyamide present potential safety and environmental risks, while poly(vinylidene fluoride) is an expensive material. Ethylene vinyl alcohol copolymers can limit diffusions of nonpolar gases like oxygen, helium, and hydrogen; however,

they can only be used in low humidity conditions, as high humidity causes the material expansion and thus increases the hydrogen permeability.<sup>57</sup> In addition, since water molecules increase plasticity and decrease the intermolecular strength of poly(vinyl alcohol), the presence of water enhances the mobility of the molecular chain segments and thus increases the number and size of channels through which the hydrogen permeates.

The hydrophilic characters of polymer materials originate from the hydrophilic groups such as hydroxyl, amine, carboxyl, etc. It was reported that ethylene is good for water impermeability but not for gas resistance, while vinyl alcohol is the opposite.<sup>19</sup> The hydrogen permeability is 600 and 4000 cm<sup>2</sup> μm/(m<sup>2</sup> day atm) when the ethylene content in ethylene vinyl alcohol copolymer is at 32 and 44 wt %, respectively. The solubility of water could be reduced with the addition of other materials such as graphene;<sup>57,58</sup> however, the cost might be a concern. Addition of other monomers such as polyethyleneimine<sup>59</sup> to form composite coatings might be another solution, which will be discussed more in sections 2.3.5 and 3.3.

Klopffer et al.<sup>60</sup> studied the hydrogen permeability on some common pipeline materials such as highly dense polyethylene (HDPE), polyamide 11 (PA11), and poly(6-amino-1-hexyl methacrylate) (PAHM). Among them, the hydrogen permeabilities of polyethylene and PA11 are  $2 \times 10^{-8}$  and  $8 \times 10^{-9}$  cm<sup>3</sup>/(cm s bar), respectively.



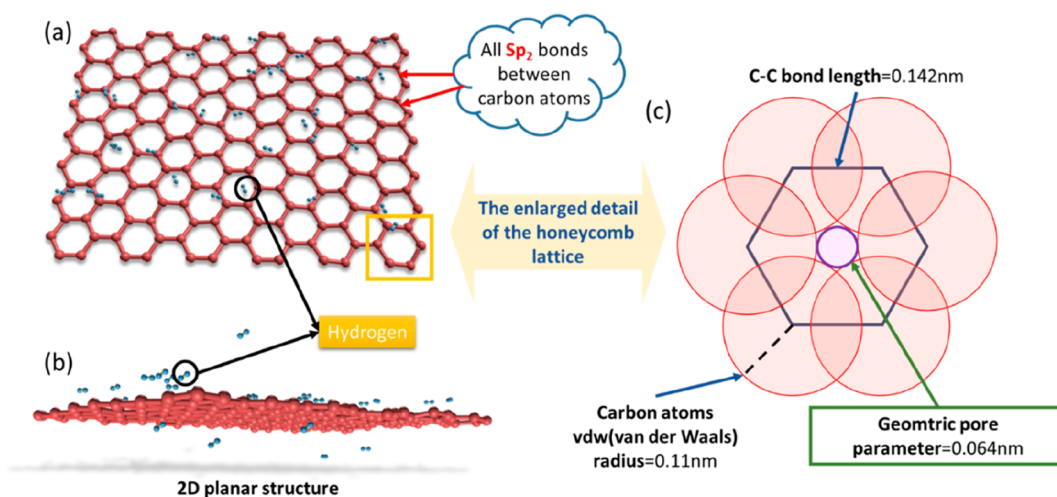


**Figure 7.** Hydrogen permeation through graphene coatings. (a) Lattice structure of graphene, (b) lateral view of hydrogen permeation on graphene coatings, and (c) enlarged detail of the honeycomb lattice.

The low price and lightweight of the polymers are attractive to researchers. However, a significant portion of polymers show better ability to block macromolecular gases like oxygen than to resist micromolecular gases like hydrogen and helium (Figure 6).<sup>61</sup> The barring ability of tested coatings for hydrogen is lower than those of oxygen and carbon dioxide.

**2.3.4. Two-Dimensional Materials.** Two-dimensional materials such as graphene and graphene-like materials have gained interest as potential coating materials, as they have advantages of being lightweight and having high chemical and thermal stability and high mechanical strength. It has been found that two-dimensional materials with a network structure and dense electron cloud distribution, although only one atom thick, have strong particle blocking properties. Two-dimensional materials are abundant in variety, such as hexagonal boron nitride (h-BN) or molybdenum disulfide ( $\text{MoS}_2$ ), but all exhibit a graphenelike structure. However, different materials have different blocking effects on hydrogen tunneling.<sup>12</sup> The overall and microstructure of graphene is shown in Figure 7, in which panel (a) shows the lattice structure of graphene:  $\text{sp}^2$  hybridized carbon atoms arranged in a 2D honeycomb lattice, (b) shows the lateral view of hydrogen permeation on the 2D planar structure of graphene coatings, and (c) shows the enlarged detail of the honeycomb lattice and the molecular structure with rough electronic density distribution. In addition to the repulsion of the electron cloud, virtually the geometric pore parameter is small enough not to allow molecules to pass through.

**2.3.4.1. Graphene.** Graphene has high chemical and thermal stability, nontoxicity, and corrosion resistance. As a two-dimensional material, graphene is composed of carbon with  $\text{sp}^2$  bonds in plane with  $\pi$  orbitals perpendicular to the surface, which connect to each other in a two-dimensional cellular lattice. The electron density on the aromatic ring is high, which repels other molecules.<sup>62</sup> Graphene has been found to block all gases, including helium and hydrogen isotopes like  $\text{D}_2$ .<sup>62</sup> At the same time, the strongly bonded structure of graphene ( $\text{C}=\text{C}$  bond energy = 4.9 eV, inherent strength = 49 N/m) makes it the thinnest waterproof film. The mechanical strength of graphene is also key to hydrogen permeation resistance, as it can withstand pressure and maintain the structure of the barrier.<sup>63</sup> By the way, the geometric pore diameter of graphene

is 0.064 nm, quite difficult for molecules to pass through (Figure 7).<sup>63</sup>

Hydrogen on graphene surface has three processes from the perspective of microscopic particle migration: hydrogen adsorption, hydrogen atom migration, and desorption of the hydrogen molecule ( $\text{H}_2$ ). Nguyen et al.<sup>64</sup> analyzed the possible hydrogen atom migration and the potential barrier in the desorption process of hydrogen atoms and molecules on the surface of monolayer graphene using the functional density theory. As a finding, it was revealed that at the stable hydrogen adsorption site, the lowest barrier for hydrogen atom desorption was 149.3 kJ/mol, and the migration barrier of hydrogen atom was higher than 191.0 kJ/mol. The high energy barrier effectively restricts the migration of hydrogen atoms. Moreover, the hydrogen molecules can only be desorbed from the edges on which the hydrogen atoms are adsorbed.

Currently the preparation process for mass production of graphene films is chemical vapor deposition. Young et al.<sup>62</sup> prepared the graphene film on the surface of copper via chemical vapor deposition, and the resulting permeation reduction factor (PRF, see section 4.2.2) was around 28. Fan et al.<sup>65</sup> also obtained the graphene film on nickel alloy through chemical vapor deposition. The current density they measured was half lower than that of the uncoated material, which proves the ability of hydrogen permeation resistance of graphene.

However, the results are not stable because it is difficult to keep the perfect structure of graphene on which the pinholes affect the hydrogen permeability. Moreover, due to the fragile mechanical property of graphene, it is a challenge to transfer graphene from its originally growing substrate onto the target substrate,<sup>66</sup> which might affect the hydrogen permeation property of coatings.

Some reports also found that graphene may corrode metal materials, and the pinholes, cracks, or scratches on coatings will accelerate this process, due to galvanic coupling between graphene and metal.<sup>67–70</sup> This matter can be solved either by adding anodic materials, such as zinc, or inserting insulating materials, such as polymer to form graphene–polymer composite coatings, to break galvanic couplings between the graphene and the metal.<sup>67</sup>

**2.3.4.2. Molybdenum Disulfide ( $\text{MoS}_2$ ).** Molybdenum disulfide ( $\text{MoS}_2$ ) is a semiconductor with a melting point of 1185 °C. The  $\text{MoS}_2$  layer usually exhibits a good adhesion

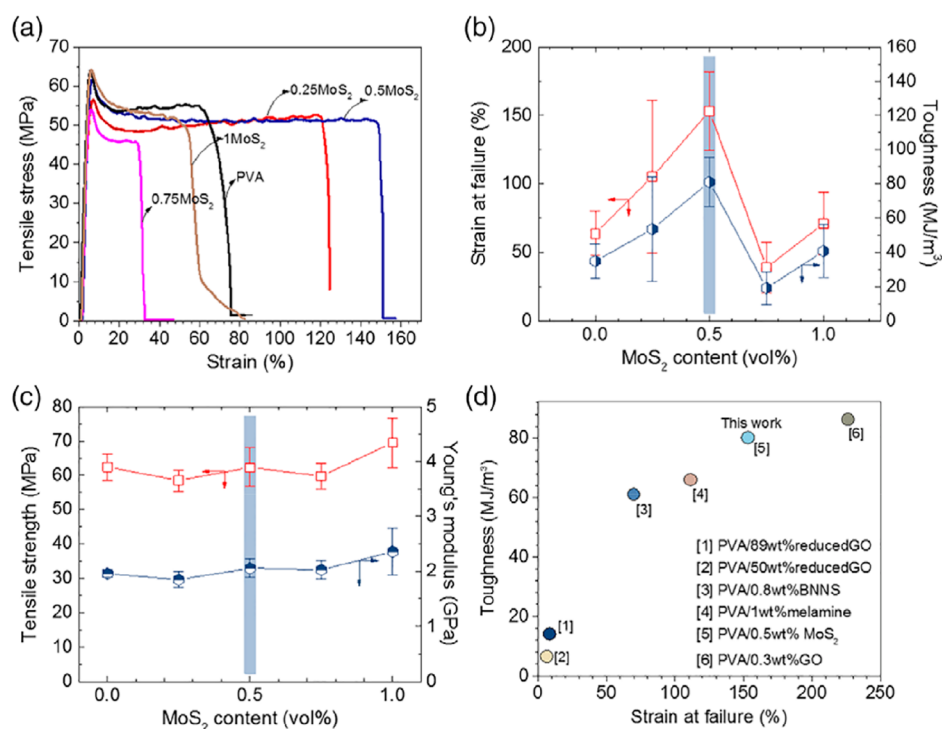


**Figure 8.** Properties of poly(vinyl alcohol) (PVA) coatings by adding different contents of 2D materials: MoS<sub>2</sub> (molybdenum disulfide) nanosheets, with (a) tensile stress versus strain curves, (b) strain at failure, (c) tensile stress at different MoS<sub>2</sub> contents, and (d) the comparison of toughness and ductility of PVA-0.5 wt % of MoS<sub>2</sub> with other PVA nanocomposites. Reprinted with permission from ref 75. Copyright 2019 John Wiley & Sons, Inc.

performance because the sulfur atom can bond tightly to a metal surface. Li et al.<sup>71</sup> analyzed the hydrogen transfer energy between a MoS<sub>2</sub> layer and an Fe (111) surface by spin-polarized density function theory (DFT). It was found that the hydrogen adsorption energy on the surface increased from 0.55 to 1.26 eV, which proves that MoS<sub>2</sub> can be used as a hydrogen barrier. Monolayered MoS<sub>2</sub> can effectively inhibit the dissociation adsorption of hydrogen molecules by forming a S–H bond.

**2.3.4.3. Hexagonal Boron Nitride (h-BN).** Hexagonal boron nitride (h-BN) has been proposed to reduce the H<sub>2</sub> diffusion into substrates at high temperatures.<sup>31</sup>

The effectiveness of thin h-BN depends on the deposition method and the resulting microstructure. The h-BN coating with (002) planes perpendicular in X-ray diffraction on substrate through ion beam-assisted deposition is extremely permeable to hydrogen, while the hydrogen permeability is drastically reduced if the deposition is processed via radio frequency magnetron sputtering.<sup>72</sup> Bull et al.<sup>31</sup> found that when h-BN flakes parallel to the substrate surface, it traps molecular hydrogen in the form of stable bubbles at 1073 K without outward diffusion. The calculation performed by the authors using density functional theory on the activation energy of hydrogen diffusion and material stability has shown us the importance of the sheet orientation parallel to the substrate surface for attaining desirable barrier film properties. Further research on the technique for how to line up the two-dimensional flakes with large domains in a correct orientation might be an attractive topic.

Overall, the hydrogen barrier energies of two-dimensional materials demonstrate that these materials are effective in hydrogen resistance. However, the research on two-dimensional

materials is still at the very beginning stage. Although such a thin film can perform a proper hydrogen resistance, the preparation technology is critical because coatings with different morphologies have totally different effects. It still needs to explore appropriate techniques to meet the different requirements for the preparation of the two-dimensional coatings.

**2.3.5. Composites.** Different coating materials have different advantages and disadvantages. Composite coatings were developed based on the existing membranes to combine their strengths and to compensate to each other's drawbacks.

**2.3.5.1. Improving the Adhesion and Enhancing the Stress.** As previously reported, alumina has poor adhesion due to the difference in thermal expansion coefficients with the stainless-steel substrate. The composite materials can significantly improve the adhesion of alumina, as revealed by many studies.<sup>34,73,74</sup>

Wu et al.<sup>40</sup> prepared a Y<sub>2</sub>O<sub>3</sub>/Cr<sub>2</sub>O<sub>3</sub> composite coating on the surface of stainless steel 316L by metal organic chemical vapor deposition, achieving a permeation reduction factor ranging from 167 to 477, higher than the pure Y<sub>2</sub>O<sub>3</sub> layer. Y<sub>2</sub>O<sub>3</sub>/Cr<sub>2</sub>O<sub>3</sub> composite coating has better hydrogen resistance and more stable permeation flux. The floating permeation reduction factor results from the distribution of the grain size. After the introduction of Cr<sub>2</sub>O<sub>3</sub>, the growth of grains obviously decrease the area between grain boundaries.

The property of the surface, such as tensile stress, Young's modulus, toughness, and strain at failure, will change when the polymer coating is mixed with other materials such as MoS<sub>2</sub> and graphene oxide (GO). Zhang et al.<sup>75</sup> found that the increasing content of MoS<sub>2</sub> in poly(vinyl alcohol) (PVA) can enhance the strain and tensile strength of the PVA coating

while they would decrease when the content of  $\text{MoS}_2$  reaches the threshold value (Figure 8).

**2.3.5.2. Preventing the Hydrogen Permeation.** Tamura et al.<sup>76,77</sup> found that hydrogen molecules could be captured by the spaces between boundaries of fine grains. The smaller the grain size, the stronger the effect. The following two cases show that the size of the grain is artificially controlled to prevent hydrogen from passing through the grain boundary.

For example, the titanium carbide layer alone has low thermal resistance and tends to oxidize easily at high temperatures. In order to improve its hydrogen barring property, Lu<sup>78</sup> prepared the  $\text{TiO}_2/\text{TiC}_x$  composite coating, with a three-step method: transplanting Ti/C atoms on the substrate, oxidation at an ultralow oxygen partial pressure, and hydrogen plasma treatment to obtain the  $\text{TiO}_2/\text{TiC}_x$  composite coating. During the heat treatment, carbon ions diffuse to both sides of the coating to form a nonstoichiometric  $\text{TiC}_x$  layer, thus providing additional hydrogen traps. The  $\text{TiO}_2$  was prepared to prevent the oxidation of titanium carbide.

Another example is that Zhou et al.<sup>79</sup> oxidized pure chromium under low pressure to obtain a single  $\text{Cr}_2\text{O}_3$  layer, then made dense bubbles on the substrate by the helium ion implantation method. A coating with helium bubbles intercepting hydrogen atoms at grain boundaries was achieved after the hydrogen plasma treatment at 500 °C, as the binding energy of the helium atom to a vacancy is much higher than that of deuterium or tritium.

**2.3.5.3. Strengthening the Hydrogen Resistance.** Pinholes are inevitably formed during the deposition of single material but can be filled with addition of other materials to form composite with improved properties. For example, Mochizuki et al.<sup>80</sup> deposited nano  $\text{Cr}_3\text{O}_2$  particles on the surface of reduced activation ferritic/martensitic steel F82H via heat treatment and then deposited  $\text{Y}_2\text{O}_3$  with metal–organic decomposition (MOD). Self-healing was achieved during this process. Expansion of the nanoparticles by oxidation was induced in the  $\text{Y}_2\text{O}_3/\text{Cr}_3\text{O}_2$  composite coating to prevent the permeation of tritium.

For the preparation of polymer materials, on the other hand, a technology called layer-by-layer self-assembly is used with exploiting the reaction between organic functional groups to form the covalent bonds and therefore to obtain a layer-by-layer structure with two or more organic materials.<sup>58,81</sup> Usually the more layers, the lower the hydrogen permeability.

**2.3.5.4. Comprehensive Utilization Improved Composite Coatings.** All above-mentioned advantages for improving adhesion, preventing hydrogen permeation, and strengthening hydrogen resistance can also be achieved simultaneously by developing suitable multilayer composite materials. Ramm et al.<sup>82</sup> and Zhang et al.<sup>43</sup> independently proposed composite coatings with three or more layers: an adhesive layer to increase the adhesion of the coating on the substrate surface, a hydrogen storage layer to capture a small amount of hydrogen passing through the hydrogen resistant layer, and a dense hydrogen-resistant layer. Park et al.<sup>83</sup> prepared a hydrogen permeation barrier in which a palladium nanolayer captures protons from the reduced  $\text{H}_2$  and traps them in a proton-rich sulfonated tetrafluoroethylene-based fluoropolymer-copolymer (so-called nafion) region by the electrical repulsive force on the interface of the positively charged polymer nanolayers. The electrons generated on the surface of palladium flow to the ground line so that the protons cannot obtain electrons to form hydrogen molecules again.

### 3. PREPARATION OF COATINGS

**3.1. Traditional Preparation Methods. 3.1.1. Physical Vapor Deposition.** Physical vapor deposition is generally carried out under vacuum conditions.<sup>84</sup> The source material is physically vaporized and then deposited to form a film on the surface of the base material.

Physical vapor deposition mainly includes radio frequency magnetron sputtering,<sup>46,49,51</sup> arc plasma plating,<sup>38</sup> and vacuum evaporation.<sup>37</sup>

Radio frequency magnetron sputtering is normally used to prepare tritium permeation barriers, where electrons collide with argon atoms within strong electromagnetic fields, thereby activating argon atoms into positive argon ions and new electrons. The argon ions accelerate toward the target cathode, bombard the target surface with high energy, causing the target materials sputtering the target atoms or molecules which deposit on the substrate surface to form a film.<sup>85</sup> The schematic drawing of radio frequency magnetron sputtering is shown in Figure 9.

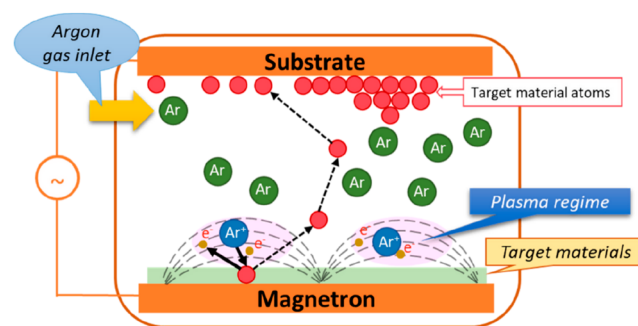


**Figure 9.** Schematic drawing of radio frequency magnetron sputtering.

Serra et al.<sup>86</sup> sputtered 1.5  $\mu\text{m}$   $\text{Al}_2\text{O}_3$  on martensitic stainless steel MANETII and successfully certified the hydrogen permeation resistance of the  $\text{Al}_2\text{O}_3$  film with the permeation reduction factor of 10000.

The coatings prepared with radio frequency magnetron sputtering are uniform, dense, and strongly bonded to the substrate, which effectively enhances the tritium-resistant performance.<sup>84</sup>

Arc plasma plating occurs in three successive steps: (1) gasifying source materials to evaporate, sublime, or sputter the plating material; (2) migration and collision of atoms, molecules, or ions from gasified sources via various reactions; and (3) deposition of atoms, molecules, and/or ions on the substrate.

The physical vapor deposition rate via arc plasma plating is high, and the film quality is good under vacuum conditions. The deposition requires a lower temperature than hot-dipping and chemical vapor deposition. The process is controlled by the plasma density, substrate temperature, bias voltage, precleaning, and the vapor composition.<sup>48</sup>

Levchuk et al.<sup>37</sup> used arc evaporation technique called pulse enhanced electron emission. This method allows continuous operation of a cathodic arc source (vacuum evaporation) in a pure oxygen environment. The achievable improvements are as follows: (1) introduction of a pretreatment: the specimens were wet chemically cleaned before entering the deposition system and then a heat-etching of the specimens was done



after the system evacuation, (2) depositing an interface consisting of Cr–Al/Cr with the thickness of about 200 nm, and (3) application of pure oxygen gas for oxidation of the interface. The permeation reduction factor obtained is in the range of 2000–3500.

**3.1.2. Chemical Vapor Deposition.** Chemical vapor deposition refers to the process in which one or more gaseous raw materials are deposited on the substrate surface via chemical reaction. The process of chemical vapor deposition is divided into the following steps: (1) the diffusion of reactive gas flow to the substrate surface, (2) the adsorption of the reactive gas flow to the substrate surface, (3) the formation of film by chemical reaction on the substrate surface, and (4) the desorption of gaseous byproducts from the substrate surface (Figure 10).<sup>87</sup>

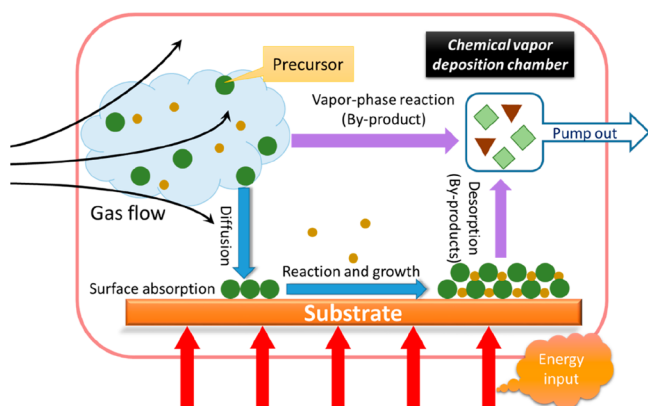


**Figure 10.** Conventional chemical vapor deposition.

Compared to physical vapor deposition, chemical vapor deposition provides excellent coating performance and is suitable for coating complex surface and internal pores. It allows for simple control of the composition and properties of synthetic coatings and thus is cost-effective and suitable for large scale of production.<sup>40</sup>

However, the high deposition temperature required by chemical vapor deposition may damage the mechanical property of substrate materials such as reduced activation martensitic steels.<sup>84</sup> The coating produced by chemical vapor deposition may have more pores and defects than by physical vapor deposition, which may meet some other challenges. For example, graphene is hard to be transferred from the metal substrate where the graphene grows up.

**3.1.3. Sol–Gel Coating.** Sol–gel coating is a wet coating technique in which a colloidal solution of metal alkoxide or inorganic salt dissolves in water after a shrinking reaction is applied to the surface of the substrate to form the final coating after drying and heat treatment. Sol–gel coating is one of the most versatile and simple techniques for the formation of thin films. It can be used in a wide range of temperatures (from 500 to 1100 °C), requires simple equipment, and allows one to obtain uniform coatings with accurate and controllable compositions.<sup>74</sup>

However, the sol–gel coating requires a long processing time. Because the combination of alcohol salts and water is used, shrinkage or cracking of the coating might occur.<sup>41</sup> Moreover, it was mentioned that this method is not suitable for preparing coatings on preoxidized substrates.<sup>84</sup>

**3.1.4. Hot Dip Aluminization.** Hot dip aluminization is a chemical heat treatment in which aluminum penetrates the surface of stainless steel to make it more resistant to oxidation and corrosion. As part of the process, the stainless substrate is firstly immersed into the molten aluminum bath to form a Fe–Al alloy layer, which is called pretreatment. The pretreatment time depends on the thickness and the diameter of the steel pipe. Hot dip aluminization is an operationally simple process. This technology can be used to prepare a tritium permeation barrier. The properties of hot dip aluminization coatings are affected by the pretreatment, oxygen concentration, and the oxidation process of the substrate. Coatings prepared on a clean and smooth substrate surface and under lower oxygen conditions have better qualities.<sup>23,45,51,88</sup>

The application of hot dip aluminization is only limited to the preparation of aluminide coatings. Once again, the technology requires a higher heat treatment temperature, which may affect the performance of the substrate.

**3.1.5. Plasma Spraying.** Plasma spraying uses a plasma arc as a heat source to heat ceramics, metals, and their alloys to a molten or semimolten state and then sprays the molten or semimolten materials onto the surface of the substrate at high speed. The coating is formed after a heat treatment.

The plasma spraying method has a high deposition rate and wide application range. However, the coatings prepared by plasma spraying are generally of low quality with low density and poor substrate bonding.<sup>86,89</sup> This drawback can be effectively overcome by adding an intermediate bonding layer or a transition layer between the coating and the substrate.<sup>90</sup> Plasma spraying combined with other methods is potentially much more efficient.<sup>48</sup>

Plasma spraying is not suitable for the preparation of special-shaped parts and their inner surface coatings. It is noted that the plasma spraying deposition process can lead to a significant increase of the temperature on the surface of the substrate which may affect the original property of the substrate.

**3.1.6. Pack Cementation.** The process of pack cementation consists of three steps:<sup>84</sup> (1) metal halide molecules, prepared by reaction of an activator (metal solid) and a penetrant (the halogen gas), diffuse on the surface of the substrate, where a substitution reaction occurs to form the active metal atoms; (2) the active atoms react with the substrate and mutually diffuse to form an alloy layer; and (3) after the subsequent heat treatment, the desired coating forms on the surface of the alloy layer.

The pack cementation process is simple, suitable for workpieces with complex shape, and promising for mass production.<sup>44</sup> For example, it was also realized that the aluminide coating has gradient structure and self-healing ability.<sup>74</sup> However, pack cementation can result in severe stress corrosion of the substrate due to the presence of chloride ions in the activator used during pack cementation. Therefore, it is necessary to develop an activator suitable for preparing tritium permeation barrier by pack cementation.

**3.1.7. Slurry Dispersion.** The slurry dispersion method consists of preparing ceramic coatings by spraying or brushing the slurry onto the metal surface at room temperature. Alternatively, the metal can be coated such that it is directly immersed into the slurry for a few times and then calcined at a certain temperature.

Habel et al.<sup>57</sup> prepared a nanocomposite barrier liner by spraying lamellar liquid with a high aspect ratio to make crystalline dispersion of silicate nanosheets, which is called Na-

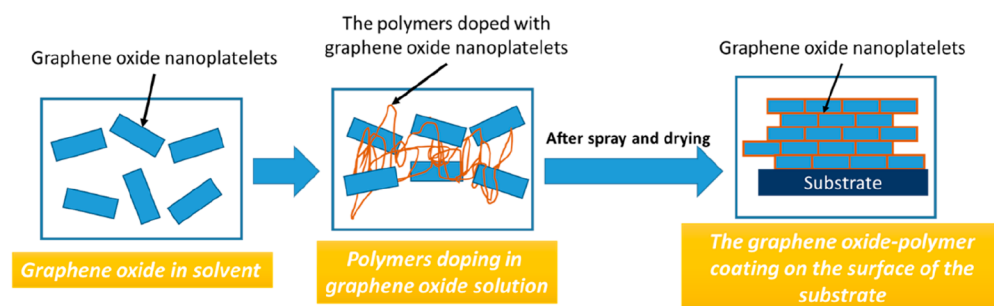


Figure 11. Preparation of graphene oxide-polymer coatings.

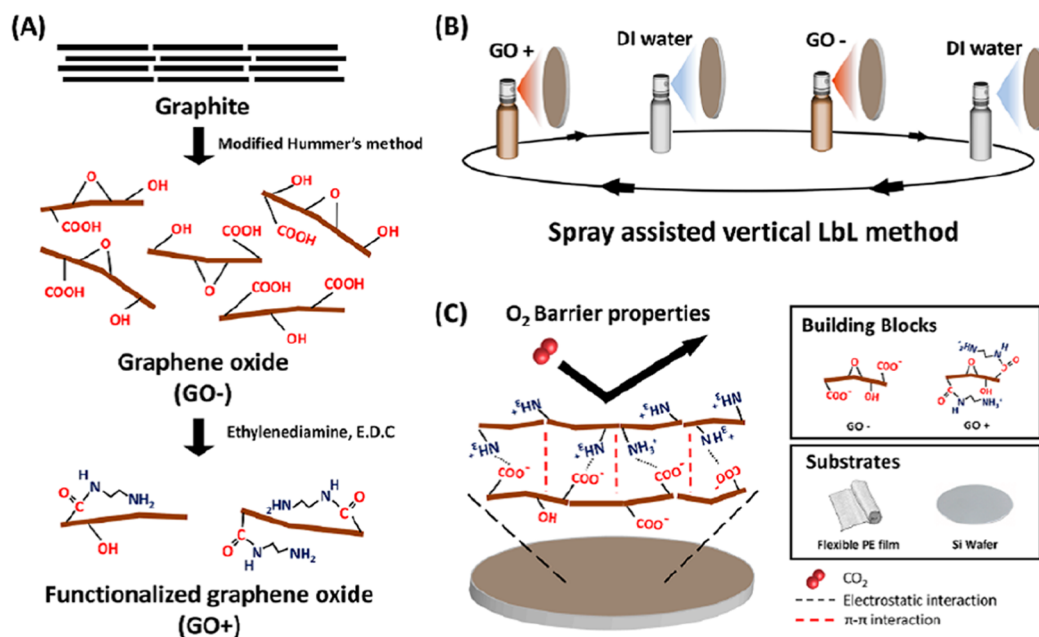


Figure 12. Schematic illustration of preparing  $\text{GO}^-/\text{GO}^+$  film by layer-by-layer self-assembly: (A) preparation of  $\text{GO}^-$  and  $\text{GO}^+$  nanosheets, (B) layer-by-layer spraying (DI water: deionized water), and (C) bonding between building blocks ( $\text{GO}^+$  and  $\text{GO}^-$  layers) as well as with substrates. Reprinted with permission from ref 96. Copyright 2019 Springer Nature.

hectorite (NaHec) nanosheets mixed with poly(vinyl alcohol) on the surface of a polyethylene glycol terephthalate foil. When Na-hectorite is immersed in alcohol or deionized water, it is layered so that the polymer hydrogen-resistant material, poly(vinyl alcohol), can combine both strengths of the Na-hectorite and polyethylene glycol terephthalate foil, and the hydrogen permeability can fall to  $0.6 \text{ cm}^3/(\mu\text{m}^2 \text{ day atm})$ . However, the results primarily profited from the high aspect ratio.

Phosphate binders are nontoxic and have well high-temperature resistance. They possess well waterproofing capability and high temperature strength because phosphate binders can be cured at low temperatures and undergo relatively limited curing shrinkage.

The slurry dispersion method is suitable for preparing tritium permeation barrier on the inner surface with a special shape or complex structure due to its fluidity.

**3.2. Preparation of Metal Compound Related Composite Coatings.** Composite coatings can be prepared by either direct or indirect methods. The direct preparation consists of directly adding one coating layer on top of another. For example, Wang et al.<sup>91</sup> coated 321 steel with a  $\text{Cr}_2\text{O}_3$  layer by electrodeposition and subsequently dipped the substrate in

$\text{AlPO}_4$  to fill the pores. The  $\text{Cr}_2\text{O}_3/\text{AlPO}_4$  coating possesses better hydrogen and corrosion resistance than pure  $\text{Cr}_2\text{O}_3$  coating. The indirect preparation consists of (1) introduction of source materials and (2) coating formation via oxidation or other reactions to fill the holes or to form a separate hydrogen-resistant layer or adherent layer.

The source materials can be introduced at different stages. (1) Addition before the coating formation: for example, Ti/C is implanted on the substrate, then oxidized under ultralow oxygen partial pressure to form a  $\text{TiO}_2/\text{TiC}_x$  structure.<sup>78</sup> (2) Addition during the coating formation: for example, silicon is added into the molten aluminum during hot dip aluminization. After the oxidation within the heat treatment, the intermetallic layer and the outer aluminum layer are transformed into a ductile phase, FeAl and  $\alpha\text{-Fe(Al)}$ .<sup>88</sup> In another sample, Liu et al.<sup>73</sup> fabricated a  $\text{Cr}_2\text{O}_3$  coating via electrodeposition (dipping into the electrolytic solution containing  $\text{Cr}_2\text{O}_3$ ) and then immersed it into the  $\text{AlPO}_4$  solution to dissolve the graphene oxide. The graphene oxide-aluminum phosphate/ $\text{Cr}_2\text{O}_3$  double coating has the character of graphene and presents better hydrogen resistance, hardness, and filled micropores. (3) Addition after the coating formation: for example,  $\text{Cr}_2\text{O}_3$  coating is prepared after the oxidation of the metal chromium,

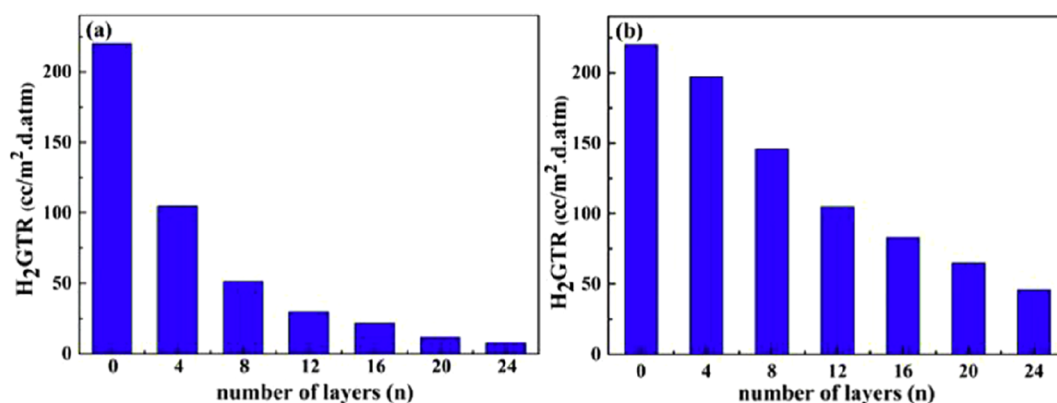


**Figure 13.** Hydrogen gas transmission rates ( $H_2GTR$ ) through layer-by-layer films formed with (a) hydrogen bond and (b) electrostatic interaction, respectively. Reprinted with permission from ref 59. Copyright 2017 Elsevier.

and then helium ions are implanted to occupy the channel to obstruct the hydrogen.<sup>79</sup>

**3.3. Preparation of Polymer and Polymer Related Composite Coatings.** Traditionally polymer coatings which have layers of barrier nanosheets are prepared such as to spray the solution containing the coating materials onto the substrate and then to evaporate the solvent to form polymer-barrier nanosheets.<sup>92,93</sup> Taking graphene oxide as an example, the graphene oxide nanoplatelet-polymer barrier coated on the substrate is described as shown in Figure 11. Except for graphene oxide, other nanoplatelets used in polymer coatings such as montmorillonoid<sup>57</sup> and laponite<sup>94</sup> were also reported. For the 2D material, h-BN, challenges including agglomeration, incompatibility, and weak interactions with the host polymers should be considered.<sup>95</sup>

The layer-by-layer assembling method is often used in preparation of polymer materials in which covalent bonds or electrostatic bonds between atoms of different layers are often formed during the assembling process. For example, in the nanosized graphene oxide ( $GO^-$ ) multilayer films, positively charged amine-functionalized  $GO^+$  was synthesized using the negatively charged  $GO^-$  dispersion, ethylenediamine, and 1-(3-dimethylaminopropyl)-3-ethylcarbodiimide methiodide (E.D.C.), as shown in Figure 12.<sup>96</sup>

Platelets formed from spraying behave like fillers. Films prepared by hydrogen bonds were considered better than electrostatic bonds because the former are weaker and thus easier for packing and overlapping in multilayered assembling.<sup>81,97–99</sup> For example, when the layer-by-layer films of montmorillonite (MMT) and polyvinylpyrrolidone (PVP) are linked by electrostatic bonds, the montmorillonite layer swells together with the polyvinylpyrrolidone layer. However, if they are linked by hydrogen bonds, when the polyvinylpyrrolidone expands, the clay layers will be virtually untouched.<sup>93</sup>

Therefore, the interactive force between nanoplatelets and polymers affects the hydrogen barring capacity. For example, Liu et al.<sup>59</sup> made the polyethyleneimine (PEI)-reduced graphene oxide (RGO)/poly sodium 4-styrenesulfonate (PSS)-RGO films through the layer-by-layer assembling method. The hydrogen transmission rate (hydrogen permeability) of the 24-layered film linked by hydrogen bonds can drop down to 5.8 mL/(m<sup>2</sup> d atm) in comparison with the one-layered polymer film, while for the film made by electrostatic interactions, it can only be reduced to 46.2 mL/(m<sup>2</sup> d atm) (Figure 13). So, the hydrogen barrier capacity of coatings

made via hydrogen bonding is better than via electrostatic interactions. It is not surprising that the more layers, the better barrier.

To achieve the dense layer morphology, polymerization parameters, including temperature, immersion time, pH, immersion angle, and solution concentration, affect the quality of the films. However, to the best of our knowledge, there is no standard or target available for the acceptance of hydrogen barriers. All we can see from Figure 13 is the more layers the better. However, it may cause other issues in addition to the cost, such as the adhesivity of the coating onto the substrate due to the difference in thermal expansion coefficients.

## 4. HYDROGEN PERMEATION EVALUATIONS

### 4.1. Factors Affecting the Effectiveness of Hydrogen Permeation.

**4.1.1. Common Factors for All Types of Coatings.** The qualities of coatings are affected by factors including the crystalline structure of the material, the surface density, the difference of thermal expansion coefficients between the coating and the substrate, the coating thickness, and the coating preparation method.

**4.1.1.1. Thermal Expansion Coefficient.** It has been confirmed in the literature that austenitic and martensitic stainless steel like 16Mn and 316L steel has excellent hydrogen resistant ability,<sup>100</sup> where 316L stainless steel is also used as the base material in most research. The thermal expansion coefficient is used as an index of adhesion. If the difference of the thermal expansion coefficients between the barrier and the stainless-steel substrate is too large, the coating on the surface of the steel may wrinkle and crack thereby forming holes as the temperature rises, bringing the hydrogen into direct contact with the substrate. Therefore, when selecting the adhesive layer, a material with good adhesion and close thermal expansion coefficient to the substrate should be chosen to keep the surface integrity of the hydrogen permeation barrier and to avoid the appearance of defects. On the other hand, if the adhesion degree of the coating and the substrate is low, it may cause the coating to peel off the surface of the steel, and thus it is difficult to form a protective barrier layer. A subtle detachment of the film may lead to the accumulation of the hydrogen and trigger the crack.

The adhesion degree of the coating and the substrate can be tested by a scratch test, acoustic emission, tangential friction, and electron probe techniques.<sup>101</sup>



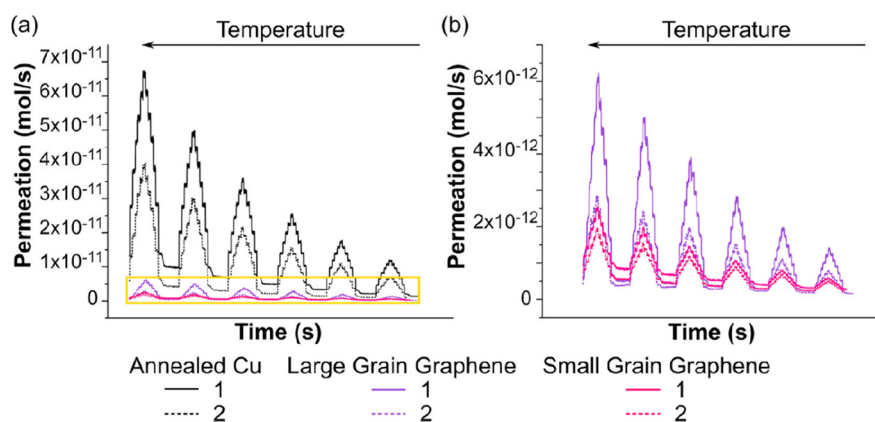


**Figure 14.** Hydrogen permeation from annealed Cu (copper) and the Cu coated by large and small grain graphene, respectively. Solid and dashed lines represent two different batches of samples. Panel (b) is the enlarged figure in the yellow box of panel (a). Reprinted with permission from ref 62. Copyright 2021 Elsevier.

**4.1.1.2. Thickness.** Generally, the effect of hydrogen resistance increases along with the thickness of the coating. However, if the coating is too thick, it may cause cracking. For some two-dimensional materials, thin film can well prevent the hydrogen permeation.

Li et al.<sup>102</sup> obtained the  $\text{Er}_2\text{O}_3$  hydrogen isotopes permeation barrier (HIPB) through magnetron sputtering. They found that 0.2 mm of  $\text{Er}_2\text{O}_3$  coating could reduce the deuterium permeation to about 1/10–1/20. The reduction ability gradually decreased along with the coating thickness when it was thicker than 0.2 mm, possibly due to the deuterium invasion in the permeation test.

**4.1.1.3. Grain Size.** As the coating layer captures hydrogen through grain boundaries, grain size and morphology play a particular role.<sup>76,77</sup> Usually the smaller grain size, the smaller the grain boundary and the surface of the coating more dense and, thus, the better the hydrogen resistance. For example,  $\text{Al}_2\text{O}_3$  film consisting of fine crystal grains with diameters below 40 nm has found a superior hydrogen-permeation barrier effect.<sup>76</sup> The microcrystalline structure with many grain boundaries is expected to provide effective hydrogen-barrier performance. Figure 14 illustrates the difference of hydrogen permeation from annealed Cu and the Cu coated by large and small grain graphene, respectively. Graphene-coated Cu materials have much smaller hydrogen permeability than copper itself (Figure 14a). Furthermore, the small-grain graphene-coated film has further lower hydrogen permeability than the one coated with large grain of graphene (Figure 14b).<sup>62</sup>

However, arguments remain that the microstructure rather than the particle size itself plays a more important role. Within the study on the relationship between deuterium permeation and the microstructure of yttrium oxide coating, Wu et al.<sup>103</sup> revealed that the permeation property of the coating is highly dependent on the microstructure. They claimed that the permeation does not depend so much on the grain size but rather on the pinholes and some cracks present on the surface of the coating. Therefore, they verified that the  $\text{Y}_2\text{O}_3/\text{Cr}_2\text{O}_3$  composite coating has better deuterium inhibition performance than the single-layered  $\text{Y}_2\text{O}_3$  coating with the same thickness, although the introduction of the  $\text{Cr}_2\text{O}_3$  layer also has the effect of enlarging the grain size of the  $\text{Y}_2\text{O}_3$  coating.<sup>40</sup> Moreover, high hydrogen permeability is expected if the grain has a columnar shape (>100 nm).<sup>77</sup>

Scanning electron microscopy (SEM) and transmission electron microscopy (TEM) are normally used to analyze the surface density. Finer surface morphology can be studied by atom force microscopy (AFM).<sup>77</sup>

**4.1.1.4. Preparation Methods.** Coating quality also varies against different preparation methods. For example, a SiC coating can be prepared either by ion beam-assisted deposition or ion implantation. Although high surface density coatings can be obtained with both methods, the hydrogen resistance efficiency of the coating prepared with the second method is higher.<sup>50</sup> When a small part of silica is generated *in situ*, the permeation reduction factor becomes 5 orders of magnitude greater than that of the original 316 stainless steel.

Su et al.<sup>104</sup> obtained defect-free monolayered graphene coating by reducing graphene oxide (GO) with both hydrogen iodide and vitamin C through vacuum filtration of a graphene oxide solution with poly(vinyl alcohol) (PVA). The hydrogen iodide reduced graphene exhibited superior impermeability, while the vitamin-C-reduced-graphene exhibited superior corrosion resistance, even in the hydrogen fluoride (HF) environment. However, this method is expensive and difficult to achieve on an industrial scale.

**4.1.2. Factors Specifically Affecting Polymers.** For coatings made from polymer materials, the intrinsic characteristics of the polymers will affect the behaviors of coatings, including the following: (1) Crystalline structure: Crystalline structure is interrelated with the density of the polymer. The hydrogen permeability of semicrystalline polymers is lower than the amorphous ones. Polymer with a more defined crystalline structure has a higher density. (2) Cross-linking: Cross-linking is the process by which the linear or branched polymer chains are covalently linked to form a network or shaped polymer, which can reduce the hydrogen permeability. (3) Molecular mass: Hydrogen permeation through a polymer normally ceases or is limited at certain molecular masses.<sup>56</sup> Polymer with the highest molecular mass generally has lower permeability. (4) Orientation: Polymer orientation refers to the polymer chains, crystal bands, wafers, grains, or fibrous filters and are arranged in order along the direction of external force, which makes the molecular bonds more tightly packed and thus improves the hydrogen resistance. (5) Addition of plasticizers: Plasticizers will improve the active capacities of chain segments and then enhance the hydrogen resistance.

The hydrogen permeation through a material depends on its preparation process and morphology selection. Like the metal coatings, polymer is easy corroded from the pinholes and fractures.<sup>105</sup> In addition to physical damages, the overall effect of permeation reduction is determined by the combination of many factors and these factors in turn influence each other. Thus, there is still a long way to go for mass production.

## 4.2. Hydrogen Permeability Evaluation Techniques.

**4.2.1. Electrochemical Evaluation.** The instrument for the electrochemical measurement of hydrogen permeability is relatively simple and inexpensive (Figure 15), which is called

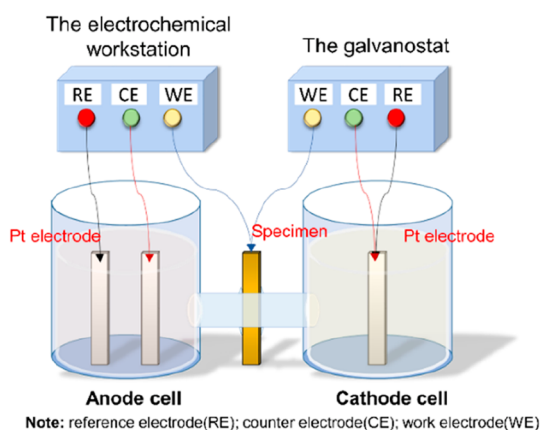


Figure 15. Electrochemical permeation measuring instrument.

Devanathan-Stachurski (D-S) cell, and the analytic results are quite accurate.<sup>18</sup> However, the surface state may not be well stabilized as the diffusion is performed at room temperature and in a long analytic time.<sup>35</sup>

In the cathode cell, on the right side of Figure 15, the hydrogen ions present (in electrolyte solution) can react with the electrons supplied on the cathode surface by a galvanostat (also known as an amperostat), forming hydrogen atoms. The atomic hydrogen passes through the tested sample (the specimen), and the hydrogen permeation current is recorded by an electrochemical workstation in the anode cell (Figure 15, left) to obtain a hydrogen permeation curve. The hydrogen diffusion coefficient can be calculated with the following equations:<sup>18</sup>

$$D = \frac{d^2}{15.3t_b} \quad (3)$$

$$D = \frac{d^2}{6t_{0.63}} \quad (4)$$

where  $D$  is the hydrogen diffusion coefficient in  $\text{m}^2/\text{s}$ ;  $d$  is the sample thickness in meters;  $t_b$  is the transferring time (the time corresponding to the intersection of the tangent line at the inflection point and the horizontal axis in the permeation curve) in seconds; and  $t_{0.63}$  is the retardation time (the time when the permeation current reaches 0.63 times the steady-state current value) in seconds. The principle of the electrochemical measurement and the parameters mentioned above in analyzing the electrochemical hydrogen permeation current curves are described in Figure 16.

The actual diffusion coefficient is slightly larger than that calculated with eqs 3 and 4 because the traps in the material capture the hydrogen entering the material until the traps are

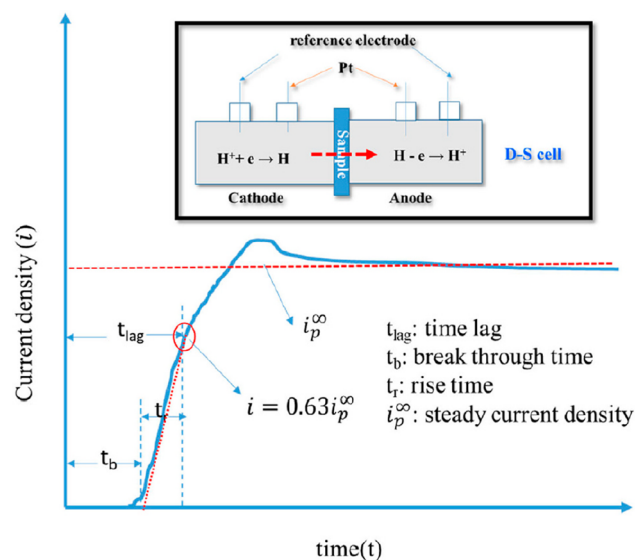


Figure 16. Schematic working principle of the Devanathan-Stachurski (D-S) cell (top) and the illustration of electrochemical hydrogen permeation current curve (bottom). Reprinted with permission from ref 106. Copyright 2022 Elsevier.

filled. If the experimental and calculated results differ too much, it indicates the existence of “short circuit” diffusion along grain boundaries.

**4.2.2. Gaseous Permeation Analysis.** The results obtained from gaseous permeation analyses are more accurate than those obtained by electrochemical tests. The following formula is used to calculate the hydrogen permeability when using gaseous permeation analysis.<sup>18,25,107</sup>

$$\text{PRF} = \frac{P_{m,\text{uncoated}}}{P_{m,\text{coated}}} \quad (5)$$

where PRF is the permeation reduction factor,  $P_{m,\text{uncoated}}$  and  $P_{m,\text{coated}}$  are hydrogen permeability before and after coating, expressed as the number of hydrogen molecules per unit area and per unit time, in  $\text{mol}/(\text{m s Pa}^2)$ .

The overall structure and working principle of hydrogen permeation testing apparatus are shown in Figure 17. There are two high vacuum chambers under different vacuum pressures on both sides of the tested material sample. The hydrogen source (Figure 17a, left side) provides hydrogen at constant pressure. The difference in pressure between the two sides induces the diffusion of hydrogen in the sample from left to right. After the desorption, hydrogen molecules enter the gas collection chamber. The hydrogen permeation flux  $J$  can be measured directly by manual operation. The instrument in Figure 17b detects the hydrogen resistance performance at different temperatures. Hydrogen permeation can be calculated with the following formula:<sup>18</sup>

$$P_m = \frac{J \times d}{P^\alpha} \quad (6)$$

where  $J$  is hydrogen permeation flux in  $\text{mol}/(\text{m}^2 \text{ s})$ ;  $P$  is the gaseous hydrogen source pressure in Pascal (Pa);  $\alpha$  is a constant referring to the existence form of hydrogen in the material, where for example,  $\alpha = \frac{1}{2}$  means hydrogen in the atomic state, while  $\alpha = 1$  refers to the hydrogen molecular form;  $P_m$  is the hydrogen permeability in  $\text{mol}/(\text{m s Pa}^\alpha)$ .

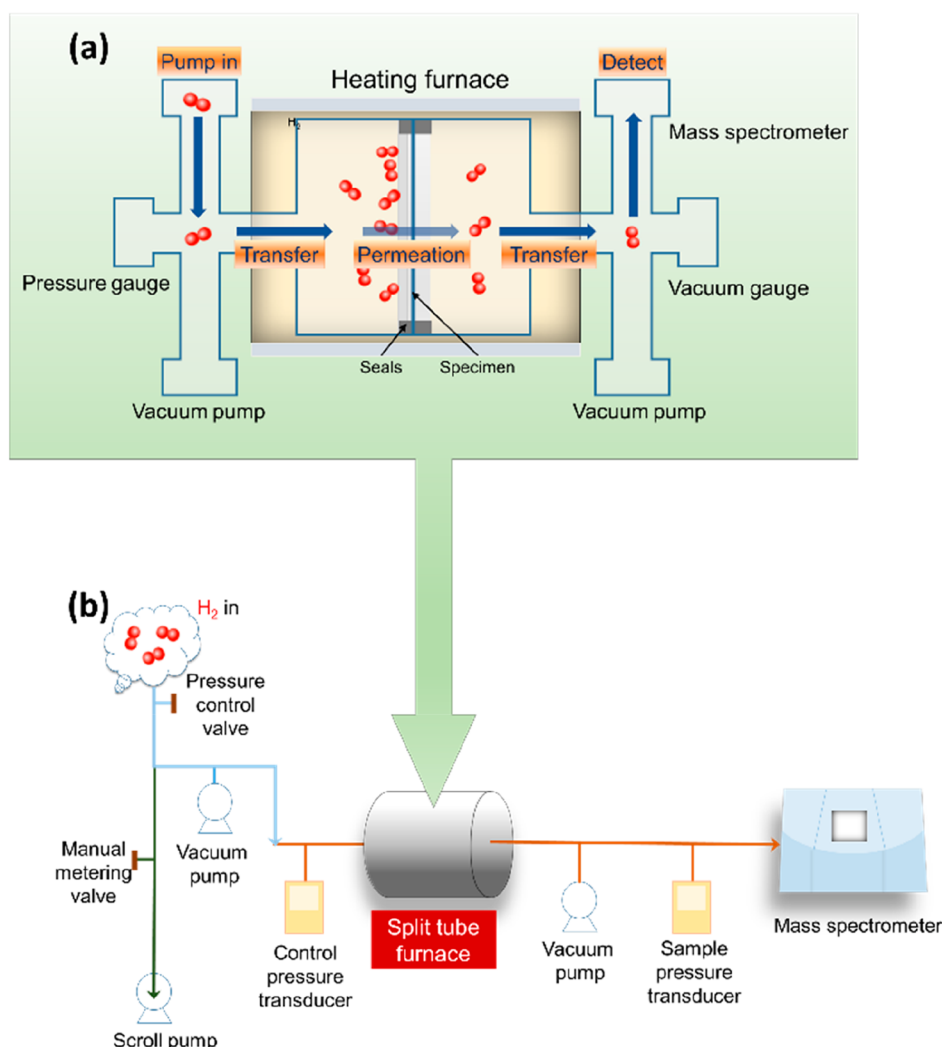


**Figure 17.** Working principle of hydrogen permeation testing apparatus with (a) hydrogen permeation chamber and (b) the hydrogen testing process diagram.

The permeation reduction factor can also be calculated using hydrogen permeation flux.<sup>25</sup>

$$\text{PRF} = \frac{J_{\text{uncoated}}}{J_{\text{coated}}} \quad (7)$$

where  $J_{\text{uncoated}}$  and  $J_{\text{coated}}$  are hydrogen permeation fluxes before and after coating, in  $\text{mol}/(\text{m}^2 \text{ s})$ .

To avoid the influence of hydrogen molecules in the gas collecting chamber during the detection of permeable hydrogen by mass spectrometer, deuterium gas is often used as the gas source.<sup>50,53,54</sup> Both pressure and temperature can be well controlled in this method.

**4.3. Permeation Reduction Factor Calculation for Composite Coatings.** The permeation reduction factor defined in eqs 5 and 7 expresses the main correlation of the hydrogen permeation barriers, although it is not sufficient to explain the true permeation mechanism. The permeation rate is always the result of the concomitance of several processes via which hydrogen passes through the film.

For the case of hydrogen permeation from pinholes and cracks, the sizes of pinholes are distributed randomly and independently. However, we can simply assume that it has identical pinholes with an average radius  $r_0$ . So, the permeation

reduction factor is only related to the exposure volume of the pinholes:<sup>107</sup>

$$\text{PRF} = \frac{\pi f \left( \frac{d_s}{r_0} \right) r_0}{4\theta d_s} = \frac{f \left( \frac{d_s}{r_0} \right)}{4nr_0 d_s} \quad (8)$$

where  $d_s$  is the thicknesses of the substrate,  $\theta = n\pi r_0^2$  represents the exposure area,  $n$  refers to the density of the pinholes;  $f \left( \frac{d_s}{r_0} \right)$  refers to a mathematical function of the ratio for the thicknesses of the substrate to the average radius of pinholes. From this formula, for the same exposure area, the finely dispersed pinholes ( $n \rightarrow \infty$ ) will nullify the barrier effect. The variables mentioned above can be described in the form of a picture as shown in Figure 18.

When the hydrogen diffusion through the film can be described with the diffusion-limited regime mechanism (DLR, defined in section 2.2), the effective permeability can be introduced with eq 9:<sup>18,25,107</sup>

$$\frac{d_s + d_f}{P_{\text{eff}}} = \frac{d_s}{P_s} + \frac{d_f}{P_f} \quad (9)$$



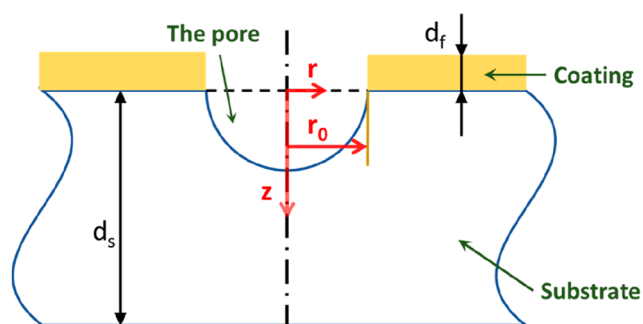


**Figure 18.** Mathematical model for hydrogen diffusion through the membrane with a single pinhole with radius  $r_0$  in the barrier film.

where  $P_{\text{eff}}$  is the effective permeability coefficient,  $d_s$  and  $d_f$  are the thicknesses and  $P_s$  and  $P_f$  are the permeability coefficients of the substrate and the film, respectively. The equation can be used when the permeation is determined by the diffusions in both layers of the doubly-layered membrane, as well as in a bare membrane. When the permeation reduction factor  $\gg 1$ , the correlation between  $P_f$  and  $P_s$  can be written as<sup>25,107</sup>

$$\text{PRF} = 1 + \frac{d_f + P_s}{d_s P_f} \quad (10)$$

$$P_f \cong \frac{d_f P_s}{d_s \times \text{PRF}} \quad (11)$$

It is much easier to determine low film permeability coefficients on high permeable substrates than on low permeable substrates, since in the latter cases the permeability easily reaches the instrumental detection limit. Some researchers have been able to obtain a reliable permeation reduction factor by working at higher test temperatures from the scheduled operation, subsequently extrapolating at lower temperatures to obtain the permeability coefficient, although this may introduce deviations.

During the hydrogen permeation process, the effective permeability is correlated with two important parameters: the diffusion coefficient  $D$  (as defined in eqs 3 and 4) and the solubility  $S$ . The solubility and the diffusion coefficient are both contained in the permeation coefficient so that they cannot be determined separately.<sup>55</sup>

$$P_{m,f} = D_f S_f \quad (12)$$

where  $P_m$  is the permeation coefficient,  $D$  is the diffusion coefficient,  $S$  is the hydrogen solubility coefficient, and  $f$  refers the film.

The time-lag coefficient  $L_t$  of the transient permeation rate can be used to define the effective diffusion coefficient:<sup>25</sup>

$$D_{\text{eff}} = \frac{(d_s + d_f)^2}{6L_t} \quad (13)$$

where  $D_{\text{eff}}$  is the effective diffusion coefficient and  $L_t$  is the observed time-lag coefficient. When the permeation reduction factor  $\gg 1$ , the following approximation is valid:<sup>25</sup>

$$\frac{D_{\text{eff}}}{D_s} = \frac{(1 + d_s/d_f)^2}{\frac{D_s}{D_f} + 3(d_s/d_f)^2} \quad (14)$$

where  $D_s$  and  $D_f$  are the diffusion coefficients of the substrate and the film, respectively.

The above equations represent the efficiency of the hydrogen permeation barrier and the corresponding properties of hydrogen permeation barrier materials.

**4.4. Calculation of Hydrogen Permeation Following a Zigzag Route on Layer-by-Layer Films with Inorganic Platelets.** The regular arrangement of nanoplatelets curing in the polymer materials forms a zigzag route. The hydrogen permeation through the layers following the zigzag route caused by a regular arrangement of nanoplatelets and the tortuous pathways are difficult for hydrogen to permeation (Figure 19).

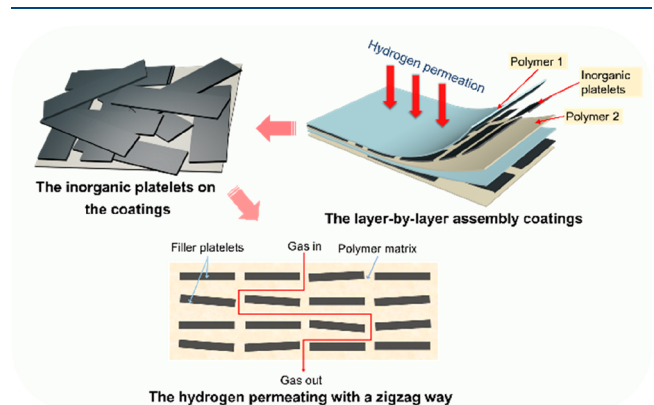


**Figure 19.** Mechanism of hydrogen permeation in the layer-by-layer assembled coating.

A parameter called tortuosity factor  $f_t$  is introduced to represent the influence of hydrogen permeability after the inorganic platelet piled on.<sup>55</sup>

$$f_t = \frac{P_m}{P_{m,0}(1 - \varphi)} \quad (15)$$

where  $f_t$  is the tortuosity factor,  $P_{m,0}$  and  $P_m$  are the permeability before and after coating, respectively, and  $\varphi$  is the volume fraction of the hydrogen pass ways. A higher tortuosity factor means a narrower route for hydrogen permeation and, therefore, a better hydrogen-resistant effect for inorganic platelets. It can also be written as<sup>55</sup>

$$\frac{P_{m,0}}{P_m} = 1 + \mu \alpha_p^2 \left( \frac{\varphi^2}{1 - \varphi} \right) \quad (16)$$

where  $\mu$  is the geometric factor of the filler, and  $\alpha_p$  is the aspect ratio of the platelets, with<sup>108</sup>

$$\alpha_p = \frac{L_p}{d_p} \quad (17)$$

where  $L_p$  and  $d_p$  are the length and the thickness of platelets, respectively.

**4.5. Other Evaluation Techniques.** In addition to the permeation reduction factor, calculated as shown in eqs 5 and 7, it is also possible to evaluate other characteristics of the prepared coating to better understand the shortcomings and potential improvements of the material. Useful indications can be obtained by carrying out measurements of suitable properties of the coating before and after the hydrogen permeation or by conducting tests under different operating conditions.

**4.5.1. Surface Morphology Analysis.** The analysis of the surface morphology is generally carried out through metallic microscope, scanning electron microscope (SEM), and atomic force microscope (AFM). These analyses supply guidance for preparing dense surface coatings.

**4.5.2. Surface Phase Analysis.** The analysis of the surface phase is determined by X-ray diffraction (XRD) and Raman spectrometry. These techniques help to understand what kind of bonds are generated during the preparation of the films, what limits the hydrogen permeation, or which phase exists to increase the hydrogen resistance. It can also indicate what is the hydrogen-resistant mechanism.

**4.5.3. Elemental Analysis.** X-ray photoelectron (XPS) and Auger electron spectroscopies (AES) are normally used to perform elemental analysis of the sample both on the surface and at different depths. The elemental ratio in the thin film may differ from the designed one. For example, the S:N ratio of silicon nitride is likely different from the ideal  $\text{Si}_3\text{N}_4$ . The abbreviation, SiN, is often applied in reference where the ideal stoichiometry is not achieved. The different elemental ratios may lead to different performances.

**4.5.4. Surface Defect Test.** Ultraviolet–visible (UV–vis) and photoluminescence (PL) spectroscopies are normally used for this kind of analysis.

**4.5.5. Coating Adhesion Test.** This includes acoustic emission, tangential friction, and electron probe techniques, etc.

**4.5.6. Element Exploration.** With regard to exploration of the fine flaws, atom probe tomography (APT) has become an advanced technology for evaluating the hydrogen atom concentration. This technique has successfully certified the feasibility of the utilization of hydrogen traps with defects like dislocations, grain boundaries, and precipitates.<sup>109</sup>

## 5. PROSPECTS

Although the polymer liner can reduce the container weight and improve the storage density, it was found that the hydrogen permeation through the liner became worse at high pressure because under the rapid decompression, damage might occur due to the internal hydrogen concentration resulting in big pressure difference.<sup>21</sup> Therefore, developing strengthened polymer liners inside the metal pipe of the container might be a proper direction to solve the hydrogen embrittlement problem.

However, the application of different coatings depends on the difference in environments. Compared with other coatings, polymer composites have lower cost, better plasticity, and are easier for scaled manufacture. However, it cannot be applied in the environment with high temperature because the polymer normally has a lower melting point than metal substrates and the aging rate of the polymer can be accelerated at high temperature. Considering the transport of the hydrogen storage tank at room temperature, the lightweight polymer and its composite coatings have an advantage and are more possible to be applied in daily life, such as hydrogen cars and hydrogen transport pipe networks. In the hostile environment, for example, extreme temperature in the nuclear power plant, metal materials, dielectrics, and their compositions are better options. In the toxic and corrosive environment, it will take carbides, nitrides, and graphene into consideration. The coating with low cost, high hydrogen permeation barring factor, and ease for manufacture is preferred in the applicable

working environment for gaseous hydrogen storage and transportation.

Although all approaches proposed above can be put in use in hydrogen storage and transportation, pores and cracks are hardly avoided during the coating process. The layer-by-layer polymer coatings have the best consistency on the surface. Therefore, considering the plasticity and fabricability of polymer molecules, polymer coatings might have more potential in hydrogen storage and transportation. However, most studies related to polymer coatings were only applied to block macromolecular gases (such as oxygen and carbon dioxide). The application for barring micromolecular gases (such as hydrogen and helium) are still in the research stage. Commercialization of polymer hydrogen barrier coatings still have a long way to go.

## 6. CONCLUSION

Hydrogen permeation through the storage material, mainly stainless steel, is a common problem which causes the embrittlement of stainless steel, reduces its lifetime, and may lead to serious risk. Introducing hydrogen permeation barring coatings onto the surface of stainless steel is the most effective solution.

In this review, the mechanisms of hydrogen permeation were investigated, and the working principles of hydrogen barriers were clarified. In comparison to the surface limited model and the areal-defect model, the composite barring model is the most popular coating type which has combined multifunctions.

The quality of the coating is influenced by many factors. On the basis of the hydrogen-resistant mechanism, to achieve low-cost hydrogen barriers, with fine grains, controlled surface, good adhesion, good hydrogen resistance, excellent anticorrosion performance, and high thermal resistance, the selection of coating materials, preparation conditions, and preparation methods of each layer need to be fully explored and improved.

In addition, the advantages and disadvantages of different hydrogen-resistant coatings are discussed, and the preparation technologies and the methods of evaluations were summarized. There are different preparation techniques even for the same type of coating, which have both advantages and disadvantages. So, preparation methods must be chosen according to the various needs and situations. Special materials require special preparation methods, which need to be further combined with other technologies. In addition, choosing a proper evaluation method can supply a trustable quantitative assessment to the quality of the hydrogen permeation barring coating materials and thus supply proper guidance to the preparation of the hydrogen-resistant coatings. However, it is noted that most of the evaluations were carried out under a low hydrogen pressure environment, while the reality is more challengable. When the high hydrogen pressure is beyond a certain limit, the hydrogen permeability may line up squarely.

Among the discussed different hydrogen permeation barrier coating types, polymers are competitive in manufacturing and plasticity and could become the main coating material in the future. Polymer composite coatings appear more suitable for mass production as they generally exhibit better formability, potential for cost reduction, as well as reasonable hydrogen-resistant performance.

## ■ ASSOCIATED CONTENT

### SI Supporting Information

The Supporting Information is available free of charge at <https://pubs.acs.org/doi/10.1021/acs.iecr.3c02259>.

All hydrogen permeation barrier materials including preparation techniques have been summarized (PDF)

## ■ AUTHOR INFORMATION

### Corresponding Authors

**Yangqiang Huang** – College of Chemistry and Chemical Engineering, Hunan University, Changsha, Hunan 410082, P.R. China; Email: [yqhuang@hnu.edu.cn](mailto:yqhuang@hnu.edu.cn)

**Chao'en Li** – CSIRO Energy, Clayton North, VIC 3169, Australia; [orcid.org/0000-0003-4233-3172](https://orcid.org/0000-0003-4233-3172); Email: [chaoen.li@csiro.au](mailto:chaoen.li@csiro.au)

**Rui Zhang** – College of Chemical Engineering, Xiangtan University, Xiangtan, Hunan 411105, P.R. China; Email: [ruizhang@xtu.edu.cn](mailto:ruizhang@xtu.edu.cn), [tange1026@163.com](mailto:tange1026@163.com)

### Authors

**Yufan Li** – College of Chemical Engineering, Xiangtan University, Xiangtan, Hunan 411105, P.R. China

**Francesco Barzagli** – ICCOM Institute, National Research Council, Sesto Fiorentino 50019 Florence, Italy; [orcid.org/0000-0002-5077-0420](https://orcid.org/0000-0002-5077-0420)

**Peng Liu** – International Cooperation Committee, China Foundation for International Studies, Beijing 100022, P.R. China

**Xiaozan Zhang** – Jinan Yuanze Environmental Protection Technology Co., Ltd., Jinan, Shandong 250101, P. R. China

**Zhao Yang** – Changsha Zhaoyuan Hydrogen Energy Technology Co., Ltd, Changsha, Hunan 410000, P. R. China

**Min Xiao** – Center for Applied Energy Research, University of Kentucky, Lexington, Kentucky 40511, United States; [orcid.org/0000-0003-2528-5586](https://orcid.org/0000-0003-2528-5586)

**Xiao Luo** – College of Chemistry and Chemical Engineering, Hunan University, Changsha, Hunan 410082, P.R. China; [orcid.org/0000-0003-2201-7586](https://orcid.org/0000-0003-2201-7586)

**He'an Luo** – College of Chemical Engineering, Xiangtan University, Xiangtan, Hunan 411105, P.R. China

Complete contact information is available at: <https://pubs.acs.org/doi/10.1021/acs.iecr.3c02259>

### Author Contributions

Y.L.: manuscript composition, revision, graphic creation, and first author; F.B.: manuscript composition; P.L.: manuscript composition, resources; X.Z.: manuscript composition; Z.Y.: manuscript composition; M.X.: manuscript composition; Y.H.: manuscript composition, cocorresponding author; X.L.: manuscript composition; C.L.: manuscript composition, revision, corresponding author; H.L.: manuscript composition; and R.Z.: conception, manuscript composition, supervision, cocorresponding author, and resources.

### Notes

This paper does not include any experiments involving human tissue.

The authors declare no competing financial interest.

## ■ ACKNOWLEDGMENTS

The Supports for the preliminary investigation from the National Natural Science Foundation of China (22008204) and Research Start-up Foundation of Xiangtan University

(21QDZ56) are fully appreciated. Funding for its publication from the Commonwealth Scientific and Industrial Research Organization (CSIRO), Australia, is also highly appreciated. The authors would like to express special thanks to Professor Guohua Chen, City University of Hong Kong, for valuable advice, fruitful discussion, and encouragement, and to Thomas Girke, CSIRO, for his support and encouragement regarding this publication.

## ■ REFERENCES

- (1) Camiola, V. D.; Farchioni, R.; Cavallucci, T.; Rossi, A.; Pellegrini, V.; Tozzini, V. Hydrogen Storage in Rippled Graphene: Perspectives from Multi-scale Simulations. *Frontiers in Materials* **2015**, *2*, 1–3.
- (2) Elberry, A. M.; Thakur, J.; Santasalo-Aarnio, A.; Larmi, M. Large-scale Compressed Hydrogen Storage as Part of Renewable Electricity Storage Systems. *Int. J. Hydrogen Energy* **2021**, *46* (29), 15671–15690.
- (3) Rahul, K.; Elby, T.; Maryam, S.; Olena, O.; Sivakumar, R.; Ananth, R.; Sousa, J. M. G.; Ferreira, A. L. C.; João Campos, G.; Jose, G. Hydrogen Storage for Energy Application. In *Hydrogen Storage*, Jianjun, L., Ed.; IntechOpen, 2012; Ch. 10.
- (4) Maeyama, Y.; Kadota, K.; Kitayama, A.; Tozuka, Y.; Yoshida, M.; Shimosaka, A.; Shirakawa, Y. Theoretical Study of the Temperature Dependent Hydrogen Storage Capacity of Pd and Ti Nanoparticles. *Int. J. Hydrogen Energy* **2017**, *42* (16), 11501–11509.
- (5) Hu, Z.; Srinivasan, M. P. Mesoporous High-surface-area Activated Carbon. *Microporous Mesoporous Mater.* **2001**, *43* (3), 267–275.
- (6) Rivard, E.; Trudeau, M.; Zaghbi, K. Hydrogen Storage for Mobility: A Review. *Materials (Basel)* **2019**, *12* (12), 1973.
- (7) Li, J.; Zhang, L.; Li, R.; Yang, X.; Zhang, T. High-pressure Gaseous Hydrogen Storage Vessels: Current Status and Prospects. *Energy Storage Science and Technology* **2021**, *10* (5), 1835–1844.
- (8) Abdalla, A. M.; Hossain, S.; Nisfindy, O. B.; Azad, A. T.; Dawood, M.; Azad, A. K. Hydrogen Production, Storage, Transportation and Key Challenges with Applications: A Review. *Energy Conversion and Management* **2018**, *165*, 602–627.
- (9) Li, J. Q.; Li, J. C.; Park, K.; Jang, S. J.; Kwon, J. T. An Analysis on the Compressed Hydrogen Storage System for the Fast-filling Process of Hydrogen Gas at the Pressure of 82 MPa. *Energies* **2021**, *14* (9), 2635.
- (10) Liang, J.; Zhang, R.; Zhao, Q.; Dong, J.; Wang, B.; Li, J. Molecular Simulation of Hydrogen Storage in Ion-exchanged Mazzite and Levyne Zeolites. *Computational and Theoretical Chemistry* **2012**, *980*, 1–6.
- (11) Wikipedia: Hydrogen embrittlement. [https://en.wikipedia.org/wiki/Hydrogen\\_embrittlement](https://en.wikipedia.org/wiki/Hydrogen_embrittlement) (accessed 2023-07-09).
- (12) Wang, M.; Niu, D.; Hu, Q.; Xin, Y.; Shi, H.; Huang, A. Progress of hydrogen permeation barrier adjusted by two-dimensional materials. *CIESC Journal* **2017**, *68*, 9–17.
- (13) Song, J.; Curtin, W. A. Atomic Mechanism and Prediction of Hydrogen Embrittlement in Iron. *Nat. Mater.* **2013**, *12* (2), 145–151.
- (14) Fowler, J. D.; Chandra, D.; Elleman, T. S.; Payne, A. W.; Verghese, K. Tritium Diffusion in Al<sub>2</sub>O<sub>3</sub> and BeO. *J. Am. Ceram. Soc.* **1977**, *60* (3–4), 155–161.
- (15) Lynch, S. Hydrogen Embrittlement Phenomena and Mechanisms. In *Stress Corrosion Cracking*, Raja, V. S., Shoji, T., Eds.; Elsevier Books, 2011; pp 90–130.
- (16) Noga, J. O.; Piercy, G. R.; Bowker, J. T. *Uses and Evaluation Methods of Potential Hydrogen Permeation Barriers for Nuclear Reactor Materials*; CEA 000 G 108; Canadian Electrical Association, 1985; [https://inis.iaea.org/collection/NCLCollectionStore/\\_Public/19/043/19043977.pdf](https://inis.iaea.org/collection/NCLCollectionStore/_Public/19/043/19043977.pdf).
- (17) Henager, C. Hydrogen Permeation Barrier Coatings. In *Materials for the Hydrogen Economy*, Jones, R. H., Thomas, G. J., Eds.; CRC Press, 2007; Chapter 8, pp 181–190



- (18) Zhou, C.; He, M.; Xiao, S.; Shi, K.; Wu, H.; Jiang, S.; Chen, G.; Wu, C. Review on Hydrogen Permeation Barrier Coatings on Stainless Steels. *Chemical Industry and Engineering Progress* **2020**, *39* (9), 3458–3468.
- (19) Maes, C.; Luyten, W.; Herremans, G.; Peeters, R.; Carleer, R.; Buntinx, M. Recent Updates on the Barrier Properties of Ethylene Vinyl Alcohol Copolymer (EVOH): A Review. *Polym. Rev.* **2018**, *58* (2), 209–246.
- (20) Rönnebro, E. C. E.; Oelrich, R. L.; Gates, R. O. Recent Advances and Prospects in Design of Hydrogen Permeation Barrier Materials for Energy Applications - A Review. *Molecules* **2022**, *27* (19), 6528.
- (21) Jin, Z.; Su, Y.; Lv, H.; Liu, M.; Li, W.; Zhang, C. Review of Decompression Damage of the Polymer Liner of the Type IV Hydrogen Storage Tank. *Polymers* **2023**, *15* (10), 2258.
- (22) Xiao, S.; Meng, X.; Shi, K.; Liu, L.; Wu, H.; Lian, W.; Zhou, C.; Lyu, Y.; Chu, P. K. Hydrogen Permeation Barriers and Preparation Techniques: A Review. *Journal of Vacuum Science & Technology A* **2022**, *40* (6), 1 DOI: 10.1116/6.0002178.
- (23) Yamabe, J.; Matsuoka, S.; Murakami, Y. Surface Coating with a High Resistance to Hydrogen Entry under High-pressure Hydrogen-gas Environment. *Int. J. Hydrogen Energy* **2013**, *38* (24), 10141–10154.
- (24) Kumar, N.; Chattaraj, D.; Ghosh, P.; Majumder, C. Microscopic Insights into Hydrogen Permeation Through a Model PdCu Membrane from First-principles Investigations. *J. Phys. Chem. C* **2018**, *122* (24), 12920–12933.
- (25) Nemanic, V. Hydrogen Permeation Barriers: Basic Requirements, Materials Selection, Deposition Methods, and Quality Evaluation. *Nuclear Materials and Energy* **2019**, *19*, 451–457.
- (26) Pasler, V.; Arbeiter, F.; Klein, C.; Klimenko, D.; Schindwein, G.; von der Weth, A. Development of a Component-level Hydrogen Transport Model with OpenFOAM and Application to Tritium Transport Inside a DEMO HCPB Breeder. *Applied Sciences* **2021**, *11* (8), 3481.
- (27) Wikipedia: Sieverts' law, [https://en.wikipedia.org/wiki/Sieverts%27\\_law#cite\\_note-1](https://en.wikipedia.org/wiki/Sieverts%27_law#cite_note-1) (accessed 2019-12-6).
- (28) Pisarev, A. Hydrogen Gas-driven Permeation through the Membrane with Asymmetric Surface Conditions. *J. Membr. Sci.* **2009**, *335* (1–2), 51–57.
- (29) Pisarev, A.; Bacherov, A. Hydrogen Gas Driven Permeation through Asymmetric Membranes in Diffusion Limited and Surface Limited Regimes: Interplay between Analytical and Numerical Calculations. *Physica Scripta T* **2004**, 124–128.
- (30) Causey, R. A.; Karnesky, R. A.; San Marchi, C. Tritium Barriers and Tritium Diffusion in Fusion Reactors. In *Comprehensive Nuclear Materials*, Konings, R. J. M., Ed.; Elsevier, 2012; pp 511–549.
- (31) Bull, S. K.; Champ, T. A.; Raj, S. V.; O'Brien, R. C.; Musgrave, C. B.; Weimer, A. W. Atomic Layer Deposited Boron Nitride Nanoscale Films Act as High Temperature Hydrogen Barriers. *Appl. Surf. Sci.* **2021**, *565*, No. 150428.
- (32) Wu, W.; Lei, X.; Zhong, S.; Sun, B.; Ouyang, C. First-principles Insights of Hydrogen Diffusion Dynamics at the  $\alpha$ -Al<sub>2</sub>O<sub>3</sub> (0001) Surface. *Appl. Surf. Sci.* **2020**, *531*, No. 147263.
- (33) Ramm, J. Apparatus with Permeation Barrier Layer. *European Patent EP2252720B1*, 2019, 1–20.
- (34) Zhang, M.; Zhao, R.; Ling, Y.; Wang, R.; Zhou, Q.; Wang, J.; Li, Y.; Zhang, Z. Preparation of Cr<sub>2</sub>O<sub>3</sub>/Al<sub>2</sub>O<sub>3</sub> Bipolar Oxides as Hydrogen Permeation Barriers by Selective Oxide Removal on SS and Atomic Layer Deposition. *Int. J. Hydrogen Energy* **2019**, *44* (23), 12277–12287.
- (35) Yang, Y. Preparation of Chromium Oxide Hydrogen Permeation Penetration Coating and its Properties. Master's thesis, Beijing Institute of Petrochemical Technology, 2018.
- (36) Stover, D.; Buchkremer, H. P.; Hecker, R. Hydrogen and Deuterium Permeation through Metallic and Surface-oxidized Chromium. *Surface & Coatings Technology* **1986**, *28* (3–4), 281–290.
- (37) Levchuk, D.; Bolt, H.; Döbeli, M.; Eggenberger, S.; Widrig, B.; Ramm, J. Al–Cr–O Thin Films as an Efficient Hydrogen Barrier. *Surf. Coat. Technol.* **2008**, *202* (20), 5043–5047.
- (38) Levchuk, D.; Levchuk, S.; Maier, H.; Bolt, H.; Suzuki, A. Erbium Oxide as a New Promising Tritium Permeation Barrier. *J. Nucl. Mater.* **2007**, *367–370*, 1033–1037.
- (39) Chikada, T.; Tanaka, T.; Yuyama, K.; Uemura, Y.; Sakurada, S.; Fujita, H.; Li, X.-C.; Isobe, K.; Hayashi, T.; Oya, Y. Crystallization and Deuterium Permeation Behaviors of Yttrium Oxide Coating Prepared by Metal Organic Decomposition. *Nuclear Materials and Energy* **2016**, *9*, 529–534.
- (40) Wu, Y.; He, D.; Li, S.; Liu, X.; Wang, S.; Jiang, L. Deuterium Permeation Properties of Y<sub>2</sub>O<sub>3</sub>/Cr<sub>2</sub>O<sub>3</sub> Composite Coating Prepared by MOCVD on 316L Stainless Steel. *Int. J. Hydrogen Energy* **2016**, *41* (18), 7425–7430.
- (41) Hatano, Y.; Zhang, K.; Hashizume, K. Fabrication of ZrO<sub>2</sub> Coatings on Ferritic Steel by Wet-chemical Methods as a Tritium Permeation Barrier. *Phys. Scr.* **2011**, *2011*, No. 014044.
- (42) Zhang, K.; Hatano, Y. Sealing of Pores in Sol–gel-derived Tritium Permeation Barrier Coating by Electrochemical Technique. *J. Nucl. Mater.* **2011**, *417* (1–3), 1229–1232.
- (43) Zhang, X.; Liu, X.; Deng, N.; Zhang, B. A hydrogen barrier of silicon carbide coated on stainless steel and its preparation. Chinese Patent, CN105525273A, 2018, 1–11.
- (44) Wang, Y.; Liu, D.; Feng, S.; Zhang, Y.; Ouyang, T.; Suo, J. Preparation of Tritium Permeation Barrier Consisting of Titanium by the Pack Cementation Method. *Surf. Coat. Technol.* **2016**, *307*, 271–277.
- (45) Checchetto, R.; Bonelli, M.; Gratton, L. M.; Miotello, A.; Sabbioni, A.; Guzman, L.; Horino, Y.; Benamati, G. Analysis of the Hydrogen Permeation Properties of TiN–TiC Bilayers Deposited on Martensitic Stainless Steel. *Surface & Coatings Technology* **1996**, *83* (1–3), 40–44.
- (46) Nemanic, V.; McGuinness, P. J.; Daneu, N.; Zajec, B.; Siketic, Z.; Waldhauser, W. Hydrogen Permeation through Silicon Nitride Films. *J. Alloys Compd.* **2012**, *539*, 184–189.
- (47) Houben, A.; Rasiński, M.; Gao, L.; Linsmeier, C. Tungsten Nitride as Tritium Permeation Barrier. *Nuclear Materials and Energy* **2020**, *24*, No. 100752.
- (48) Tamura, M.; Noma, M.; Yamashita, M. Characteristic Change of Hydrogen Permeation in Stainless Steel Plate by BN Coating. *Surf. Coat. Technol.* **2014**, *260*, 148–154.
- (49) Qamar, A.; Mahmood, A.; Sarwar, T.; Ahmed, N. Synthesis and Characterization of Porous Crystalline SiC Thin Films Prepared by Radio Frequency Reactive Magnetron Sputtering Technique. *Appl. Surf. Sci.* **2011**, *257* (15), 6923–6927.
- (50) Wang, P.; Liu, J.; Wang, Y.; Shi, B. Investigation of SiC Films Deposited onto Stainless Steel and their Retarding Effects on Tritium Permeation. *Surf. Coat. Technol.* **2000**, *128–129* (1), 99–104.
- (51) Wu, Y.; Zhu, S.; Zhang, Y.; Liu, T.; Rao, Y.; Luo, L.; Wang, Q. The Adhesion Strength and Deuterium Permeation Property of SiC Films Synthesized by Magnetron Sputtering. *Int. J. Hydrogen Energy* **2016**, *41* (25), 10827–10832.
- (52) Chikada, T.; Suzuki, A.; Terai, T. Deuterium Permeation and Thermal Behaviors of Amorphous Silicon Carbide Coatings on Steels. *Fusion Eng. Des.* **2011**, *86* (9–11), 2192–2195.
- (53) Liu, Y. Vanadium Carbide Coating as Tritium Permeation Barrier: A DFT Study. Master's Thesis, Dalian University of Technology, 2020.
- (54) Liu, Y.; Huang, S.; Ding, J.; Yang, Y.; Zhao, J. Vanadium Carbide Coating as Hydrogen Permeation Barrier: A DFT Study. *Int. J. Hydrogen Energy* **2019**, *44* (12), 6093–6102.
- (55) Tsurko, E. *High Barrier Waterborne Polymer-clay Nanocomposites*; University of Bayreuth: Bayreuth, 2018, <https://epub.uni-bayreuth.de/id/eprint/3563/>.
- (56) Chen, X.; Fu, Y.; Li, B. Development of Hydrogen Barrier Polymers Used In ICF. *Materials Reports (Chinese)* **2001**, *15* (3), 44–45.

- (57) Habel, C.; Tsurko, E. S.; Timmins, R. L.; Hutschreuther, J.; Kunz, R.; Schuchardt, D. D.; Rosenfeldt, S.; Altstadt, V.; Breu, J. Lightweight Ultra-high-barrier Liners for Helium and Hydrogen. *ACS Nano* **2020**, *14* (6), 7018–7024.
- (58) Tzeng, P.; Lugo, E. L.; Mai, G. D.; Wilhite, B. A.; Grunlan, J. C. Super Hydrogen and Helium Barrier with Polyelectrolyte Nanobrick Wall Thin Film. *Macromol. Rapid Communication* **2015**, *36* (1), 96–101.
- (59) Liu, H.; Bandyopadhyay, P.; Kshetri, T.; Kim, N. H.; Ku, B.-C.; Moon, B.; Lee, J. H. Layer-by-layer Assembled Polyelectrolyte-decorated Graphene Multilayer Film for Hydrogen Gas Barrier Application. *Composites Part B: Engineering* **2017**, *114*, 339–347.
- (60) Klopffer, M.-H.; Berne, P.; Espuche, E. Development of Innovating Materials for Distributing Mixtures of Hydrogen and Natural Gas. Study of the Barrier Properties and Durability of Polymer Pipes. *Oil Gas Sci. Technol.* **2015**, *70* (2), 305–315.
- (61) Yang, Y.-H.; Bolling, L.; Priolo, M. A.; Grunlan, J. C. Super Gas Barrier and Selectivity of Graphene Oxide-polymer Multilayer Thin Films. *Adv. Mater.* **2013**, *25* (4), 503–508.
- (62) Young, K. T.; Smith, C.; Krentz, T. M.; Hitchcock, D. A.; Vogel, E. M. Graphene Synthesized by Chemical Vapor Deposition as a Hydrogen Isotope Permeation Barrier. *Carbon* **2021**, *176*, 106–117.
- (63) Berry, Vikas. Impermeability of Graphene and its Applications. *Carbon* **2013**, *62*, 1–10.
- (64) Nguyen, H. T.; Huynh, L. K.; Truong, T. N. Migration and Desorption of Hydrogen Atom and Molecule on/from Graphene. *Carbon* **2017**, *121*, 248–256.
- (65) Fan, Y.; Huang, Y.; Cui, B.; Zhou, Q. Graphene Coating on Nickel as Effective Barriers against Hydrogen Embrittlement. *Surf. Coat. Technol.* **2019**, *374*, 610–616.
- (66) Langston, X.; Whitener, K. E., Jr. Graphene Transfer: A Physical Perspective. *Nanomaterials (Basel)* **2021**, *11* (11), 2837.
- (67) Cui, C.; Lim, A. T. O.; Huang, J. A Cautionary Note on Graphene Anti-corrosion Coatings. *Nat. Nanotechnol* **2017**, *12* (9), 834–835.
- (68) Xu, Y.; Qu, J.; Shen, Y.; Feng, W. Different Graphene Layers to Enhance or Prevent Corrosion of Polycrystalline Copper. *RSC Adv.* **2018**, *8* (27), 15181–15187.
- (69) Jo, M.; Lee, H. C.; Lee, S. G.; Cho, K. Graphene as a Metal Passivation Layer: Corrosion-accelerator and Inhibitor. *Carbon* **2017**, *116*, 232–239.
- (70) Sun, W.; Wang, L.; Wu, T.; Wang, M.; Yang, Z.; Pan, Y.; Liu, G. Inhibiting the Corrosion-promotion Activity of Graphene. *Chem. Mater.* **2015**, *27* (7), 2367–2373.
- (71) Li, X.; Chen, L.; Liu, H.; Shi, C.; Wang, D.; Mi, Z.; Qiao, L. Prevention of Hydrogen Damage Using MoS<sub>2</sub> Coating on Iron Surface. *Nanomaterials* **2019**, *9* (3), 382.
- (72) Checchetto, R.; Chayahara, A.; Horino, H.; Miotello, A.; Fujii, K. A Study of Deuterium Permeation through Thin BN Films. *Thin Solid Films* **1997**, *299* (1–2), 5–9.
- (73) Liu, W.; Xue, L.; Di, J.; Zhou, Q.; Zhang, H.; Li, H.; Yan, Y. An Efficient Graphene Oxide Reinforced Aluminum Phosphate/Cr<sub>2</sub>O<sub>3</sub> Double Coating as an Enhanced Tritium Permeation Barrier. *Surf. Coat. Technol.* **2021**, *405*, No. 126699.
- (74) Feng, S.; Wang, Y.; Zhang, C.; Luo, C.; Xu, J.; Suo, J. Preparation of Al<sub>2</sub>O<sub>3</sub>/Cr<sub>2</sub>O<sub>3</sub> Tritium Permeation Barrier with Combination of Pack Cementation and Sol–gel Methods. *Fusion Eng. Des.* **2018**, *131*, 1–7.
- (75) Zhang, J.; Lei, W.; Schutz, J.; Liu, D.; Tang, B.; Wang, C. H.; Wang, X. Improving the Gas Barrier, Mechanical and Thermal Properties of Poly(vinyl alcohol) with Molybdenum Disulfide Nanosheets. *J. Polym. Sci., Part B: Polym. Phys.* **2019**, *57* (7), 406–414.
- (76) Tamura, M.; Eguchi, T. Nanostructured Thin Films for Hydrogen-permeation Barrier. *Journal of Vacuum Science & Technology A: Vacuum, Surfaces, and Films* **2015**, *33* (4), No. 041503.
- (77) Tamura, M. Hydrogen Permeation Characteristics of TiN-coated Stainless Steels. *Journal of Materials Science and Engineering A* **2015**, *5* (6), 197–201.
- (78) Lu, Z.; Zhou, Q.; Ling, Y.; Hou, B.; Wang, J.; Zhang, Z. Preparation and Hydrogen Penetration Performance of TiO<sub>2</sub>/TiCx Composite Coatings. *Int. J. Hydrogen Energy* **2020**, *45* (27), 14048–14061.
- (79) Zhou, Q.; Ling, Y.; Lu, Z.; Zhang, M.; Zhang, Z.; Xiao, T.; Wang, R. Effect of Helium Implantation on the Hydrogen Retention of Cr<sub>2</sub>O<sub>3</sub> Films Formed in an Ultra-low Oxygen Environment. *Int. J. Hydrogen Energy* **2019**, *44* (48), 26685–26697.
- (80) Mochizuki, J.; Horikoshi, S.; Oya, Y.; Chikada, T. Deuterium Permeation Behavior of Tritium Permeation Barrier Coating Containing Carbide Nanoparticles. *Fusion Eng. Des.* **2017**, *124*, 1073–1076.
- (81) Li, P.; Chen, K.; Zhao, L.; Zhang, H.; Sun, H.; Yang, X.; Kim, N. H.; Lee, J. H.; Niu, Q. J. Preparation of Modified Graphene Oxide/Polyethyleneimine Film with Enhanced Hydrogen Barrier Properties by Reactive Layer-by-layer Self-assembly. *Composites Part B: Engineering* **2019**, *166*, 663–672.
- (82) Ramm, J. Permeation Barrier Layer. France EP2 252720B1, 2019.
- (83) Park, M.; Kim, D.-Y.; Kang, D.-G.; Yoon, W.-J.; Choi, Y.-J.; Lee, J. H.; Jeong, K.-U. Multilayer Thin Films for the Construction of Active Repulsive Hydrogen Barriers. *Journal of Materials Chemistry A* **2018**, *6* (6), 2456–2460.
- (84) Luo, L.-M.; Liu, Y.-L.; Liu, D.-G.; Zheng, L.; Wu, Y.-C. Preparation Technologies and Performance Studies of Tritium Permeation Barriers for Future Nuclear Fusion Reactors. *Surf. Coat. Technol.* **2020**, *403*, No. 126301.
- (85) Engels, J.; Houben, A.; Rasinski, M.; Linsmeier, C. Hydrogen Saturation and Permeation Barrier Performance of Yttrium Oxide Coatings. *Fusion Eng. Des.* **2017**, *124*, 1140–1143.
- (86) Serra, E.; Kelly, P. J.; Ross, D. K.; Arnell, R. D. Alumina Sputtered on MANET as an Effective Deuterium Permeation Barrier. *J. Nucl. Mater.* **1998**, *257* (2), 194–198.
- (87) van Deelen, J.; Illiberi, A.; Kniknie, B.; Beckers, E. H. A.; Simons, P. J. P. M.; Lankhorst, A. Atmospheric Pressure Chemical Vapor Deposition of ZnO: Process Modeling and Experiments. *Thin Solid Films* **2014**, *555*, 163–168.
- (88) Han, S.; Li, H.; Wang, S.; Jiang, L.; Liu, X. Influence of Silicon on Hot-dip Aluminizing Process and Subsequent Oxidation for Preparing Hydrogen/Tritium Permeation Barrier. *Int. J. Hydrogen Energy* **2010**, *35* (7), 2689–2693.
- (89) Fazio, C.; Stein-Fechner, K.; Serra, E.; Glasbrenner, H.; Benamati, G. Investigation on the Suitability of Plasma Sprayed Fe–Cr–Al Coatings as Tritium Permeation Barrier. *J. Nucl. Mater.* **1999**, *273* (3), 233–238.
- (90) Gao, J.; Zhang, D.; Suo, J. Tritium Permeation Barrier Based on Self-healing Composite Materials. *Fusion Eng. Des.* **2010**, *85* (7–9), 1618–1623.
- (91) Wang, Y.; Di, J.; Xue, L.; Zhang, H.; Li, H.; Yan, Y. Fabrication and Characterization of a Dense Cr<sub>2</sub>O<sub>3</sub>-Al Phosphate Double Coating as Tritium Permeation Barrier. *Fusion Eng. Des.* **2017**, *125*, 127–133.
- (92) Xue, D.; Meng, Q. B.; Lu, Y. X.; Liang, L.; Wei, Y. H.; Liu, X. B. Achieving High Performance Anticorrosive Coating via in situ Polymerization of Polyurethane and Poly(propylene oxide) Grafted Graphene Oxide Composites. *Corros. Sci.* **2020**, *176*, No. 109055.
- (93) Ding, F.; Liu, J.; Zeng, S.; Xia, Y.; Wells, K. M.; Nieh, M.-P.; Sun, L. Biomimetic Nanocoatings with Exceptional Mechanical, Barrier, and Flame-retardant Properties from Large-scale One-step Coassembly. *Science Advances* **2017**, *3* (7), No. e1701212.
- (94) Ren, W.; Wu, R.; Guo, P.; Zhu, J.; Li, H.; Xu, S.; Wang, J. Preparation and Characterization of Covalently Bonded PVA/Laponite/HAPI Nanocomposite Multilayer Freestanding Films by Layer-by-layer Assembly. *J. Polym. Sci., Part B: Polym. Phys.* **2015**, *53* (8), 545–551.
- (95) Rasul, M. G.; Kiziltas, A.; Arfaei, B.; Shahbazian-Yassar, R. 2D Boron Nitride Nanosheets for Polymer Composite Materials. *npj 2D Materials and Applications* **2021**, *5* (1), 1–18.

(96) Heo, J.; Choi, M.; Hong, J. Facile Surface Modification of Polyethylene Film via Spray-assisted Layer-by-layer Self-assembly of Graphene Oxide for Oxygen Barrier Properties. *Sci. Rep.* **2019**, *9* (1), 2754.

(97) Holder, K. M.; Priolo, M. A.; Secrist, K. E.; Greenlee, S. M.; Nolte, A. J.; Grunlan, J. C. Humidity-responsive Gas Barrier of Hydrogen-bonded Polymer–clay Multilayer Thin Films. *J. Phys. Chem. C* **2012**, *116* (37), 19851–19856.

(98) Ebina, T.; Ishii, R.; Aizawa, T.; Yoshida, H. Development of Clay-based Film and its Application to Gas Barrier Layers of Composite Tanks. *Journal of the Japan Petroleum Institute* **2017**, *60* (3), 121–126.

(99) Cho, C.; Xiang, F.; Wallace, K. L.; Grunlan, J. C. Combined Ionic and Hydrogen Bonding in Polymer Multilayer Thin Film for High Gas Barrier and Stretchiness. *Macromolecules* **2015**, *48* (16), 5723–5729.

(100) Zhai, J.; Xu, T.; Wang, H.; Ma, G.; Shang, X. The High Pressure Hydrogen Embrittlement Research of 316L and 16Mn. *Materials Reports* **2019**, *33*, 497–500.

(101) Ding, W.; Qian, C.; Chen, Y.; Wang, C.; Meng, F. Methods of Measurement and Evaluation of Adhesion Force between Film and Base Body. *Modern vehicle power* **2014**, *4*, 55–58.

(102) Li, Q.; Wang, J.; Xiang, Q.-Y.; Tang, T.; Rao, Y.-C.; Cao, J.-L. Thickness Impacts on Permeation Reduction Factor of Er<sub>2</sub>O<sub>3</sub> Hydrogen Isotopes Permeation Barriers Prepared by Magnetron Sputtering. *Int. J. Hydrogen Energy* **2016**, *41* (4), 3299–3306.

(103) Wu, Y.; He, D.; Li, S.; Liu, X.; Wang, S.; Jiang, L. Microstructure Change and Deuterium Permeation Behavior of the Yttrium Oxide Coating Prepared by MOCVD. *Int. J. Hydrogen Energy* **2014**, *39* (35), 20305–20312.

(104) Su, Y.; Kravets, V. G.; Wong, S. L.; Waters, J.; Geim, A. K.; Nair, R. R. Impermeable Barrier Films and Protective Coatings Based on Reduced Graphene Oxide. *Nat. Commun.* **2014**, *5*, 1–10.

(105) Ramezanzadeh, B.; Ghasemi, E.; Mahdavian, M.; Changizi, E.; Mohamadzadeh Moghadam, M. H. Covalently-grafted Graphene Oxide Nanosheets to Improve Barrier and Corrosion Protection Properties of Polyurethane Coatings. *Carbon* **2015**, *93*, 555–573.

(106) Liu, L.; Ruan, Q.; Xiao, S.; Meng, X.; Huang, C.; Wu, Y.; Fu, R. K. Y.; Chu, P. K. Fabrication and Hydrogen Permeation Resistance of Dense CrN Coatings. *Surf. Coat. Technol.* **2022**, *437*, No. 128326.

(107) Zajec, B. Hydrogen Permeation Barrier – Recognition of Defective Barrier Film from Transient Permeation Rate. *Int. J. Hydrogen Energy* **2011**, *36* (12), 7353–7361.

(108) Zhao, L.; Yuan, B.; Geng, Y.; Yu, C.; Kim, N. H.; Lee, J. H.; Li, P. Fabrication of Ultrahigh Hydrogen Barrier Polyethyleneimine/Graphene Oxide Films by LBL Assembly Fine-tuned with Electric Field Application. *Composites Part A: Applied Science and Manufacturing* **2015**, *78*, 60–69.

(109) Chen, Y.-S.; Lu, H.; Liang, J.; Rosenthal, A.; Liu, H.; Sneddon, G.; McCarroll, I.; Zhao, Z.; Li, W.; Guo, A.; Cairney, J. M. Observation of Hydrogen Trapping at Dislocations, Grain Boundaries, and Precipitates. *Science* **2020**, *367* (6474), 171–175.